



High Power/Energy Optics

By Prof. Victor V. Apollonov

Introduction- History of high power/energy optics is inextricably associated with the creation of a single-mode CO₂ laser ($P = 1.2$ kW), operating in the master oscillator-power amplifier regime and employing the principle of a quasi-optical transmission line, at the Laboratory of Oscillations of the P.N. Lebedev Physics Institute headed at that time by A.M. Prokhorov. Its creator was A.I. Barchukov, who worked with a team of young scientists on the problem of scaling of single-mode electric-discharge laser systems [1–5]. Due to the research conducted on such a laser system, we managed to study many physical phenomena occurring when high intensity radiation interacts with matter, including with the elements of the optical path of laser systems, which subsequently greatly facilitated creation of high-power lasers. Then, in the early 1970s, we paid attention to a phenomenon that was to limit undoubtedly the further growth of the power generated by lasers being developed [6]. More than twenty years of fundamental and applied research devoted to the study of this phenomenon and to the solution of problems associated with it allow a conclusion that its essence consists in the following. An optical surface of a highly reflecting power/energy optics element (POE) or any element of an optical path does not fully reflect radiation falling on it. A small portion of energy (fractions of a percent, depending on the wavelength) is absorbed by this reflecting element and turns into heat.

GJSFR-A Classification: FOR Code: 020599



Strictly as per the compliance and regulations of:



High Power/Energy Optics

Prof. Victor V. Apollonov

I. INTRODUCTION

History of high power/energy optics is inextricably associated with the creation of a single-mode CO₂ laser ($P = 1.2$ kW), operating in the master oscillator-power amplifier regime and employing the principle of a quasi-optical transmission line, at the Laboratory of Oscillations of the P.N. Lebedev Physics Institute headed at that time by A.M. Prokhorov. Its creator was A.I. Barchukov, who worked with a team of young scientists on the problem of scaling of single-mode electric-discharge laser systems [1–5]. Due to the research conducted on such a laser system, we managed to study many physical phenomena occurring when high intensity radiation interacts with matter, including with the elements of the optical path of laser systems, which subsequently greatly facilitated creation of high-power lasers. Then, in the early 1970s, we paid attention to a phenomenon that was to limit undoubtedly the further growth of the power generated by lasers being developed [6]. More than twenty years of fundamental and applied research devoted to the study of this phenomenon and to the solution of problems associated with it allow a conclusion that its essence consists in the following. An optical surface of a highly reflecting power/energy optics element (POE) or any element of an optical path does not fully reflect radiation falling on it. A small portion of energy (fractions of a percent, depending on the wavelength) is absorbed by this reflecting element and turns into heat. As the output power increases, even a small amount of it is sufficient to induce thermal stresses in a POE. Thermal stresses distort the geometry of the reflecting surface, affecting thereby, for example, the possibility of long-distance delivery of radiation and its concentration in a small volume. The discovered effect of thermal deformations of a POE required a theoretical study of the problem that had not been solved in such a setting ever before. Very useful was the experience in solving the problems of thermo elasticity, gained by the theoretical department headed at that time at by B.L. Indenbom at the Institute of Crystallography, USSR Academy of Sciences. Minimisation of the thermoelastic response of the optical surface of the POE exposed to intense laser radiation is one of the key problems of power optics. Improving the efficiency of laser systems, increasing the output power/energy and imposing stricter requirements to the directivity of generated radiation fluxes are inextricably linked with the need to design and create a POE with

elastic distortions $\lambda_0/10 - \lambda_0/20$ (λ_0 is the wavelength) at specific radiation loads up to several tens of kW cm⁻² [7–10].

Interest in high power/energy optics and its physical, technical and technological solutions is unabated to this day. An almost simultaneous creation of first lasers in the USA and the USSR gave birth to annual symposia on Optical Materials for High-Power Lasers (Boulder, USA) and Nonresonant Laser-Matter Interaction (Leningrad, USSR). Regular meetings of scientists and engineers, as well as proceedings of the symposia have had a significant impact on the development of research in the field of power optics in many countries [11–13].

The data presented in this review allow one to reconsider important aspects of temperature fields, thermoelastic stresses and thermal deformations in POEs, resulting from the exposure of their surfaces to high power/energy laser radiation. In this case, use is made of the relations (which are similar to Duhamel's integral formula from the theory of heat conduction) between the quantities characterising the thermal stress state in any nonstationary regimes of energy input into a solid. A peculiar feature of the analysis of the thermal stress state in this case consists in the fact that these relations comprise time t not as an independent variable, which is used in the differentiation (as, for example, in review [14]) but as a parameter, which is a consequence of incoherence of the quasi-stationary problem of thermoelasticity presented below. Thus, by using the theory we developed in the early 1970s, we consider in this review a wide range of phenomena related to the thermal stress state of a solid-body surface exposed to radiation arbitrarily varying in time [15–21]. This consideration is particularly important for the optics of high power/energy, high-pulse repetition rate laser systems that are being actively developed. The review published [14] contains data (important for the development of high power/energy optics) on the use of capillary porous structures with a different degree of the surface development, which can be efficiently employed to increase the heat exchange at a temperature below the boiling point of the coolant. The evaporation–condensation mechanism of heat transfer in the POE on the basis of porous structures and the idea of lowering the boiling temperature under reduced pressure of the coolant in cellular materials, developed by us at the same time [14, 21], are not considered in this review.

Author: A.M. Prokhorov GPI RAS, Vavilov str.38, 119991, Moscow, Russia. e-mail: vapollo@kapella.gpi.ru

II. STATIC POES BASED ON MONOLITHIC MATERIALS

Consider the most important aspects of the problem of static POE fabrication, namely, the conditions needed to achieve high optical damage thresholds for a mirror surface. Note that in our first studies [4–9] we obtained only stationary expression for the limiting intensities, leading to the optical destruction of POEs, and the stability parameters of optical surfaces based on them.

a) *Thermal stress state of a solid body exposed to laser radiation*

i. *Temperature field*

We considered a strongly absorbing isotropic body, which at the initial moment of time has a fixed temperature. The body surface with the absorption coefficient A is exposed to an axisymmetric radiation flux of arbitrary temporal shape. It is assumed that the intensity distribution in the laser beam cross section obeys the Gaussian law: $I(r) = I_0 \exp(-K_0 r^2)$, where $K_0 = 2/r_0^2$. Energy absorption takes place directly on the irradiated surface. Physically, this means that the skin-layer depth δ is smaller than the depth of the temperature field penetration in the body under consideration during the characteristic times τ of changes in the radiation intensity, i.e., $\delta \ll \sqrt{a^2 \tau}$, where a^2 is the thermal diffusivity of the material.

$$T(r, z, t) = T^* \frac{I_0 A}{2\lambda \sqrt{K_0}},$$

$$T^* = \frac{1}{2\pi i \sqrt{K_0}} \int_{\sigma-i\infty}^{\sigma+i\infty} dp \Psi(p) \exp(pt) \int_0^\infty \xi \frac{\exp(-\xi^2/4K_0)}{\gamma} \exp(-yz) J_0(\xi r) d\xi, \quad (3)$$

where p and ξ are the parameters of Laplace and Hankel transforms; $\gamma^2 = p/a^2 + \xi^2$; $\Psi(p)$ is the Laplace transform of $f(t)$; and J_0 is the zero-order Bessel function.

This expression allows us to describe the thermal state of a solid body heated by laser radiation, whose intensity varies with time in an arbitrary manner.

$$\mu \nabla^2 u + (\lambda' + \mu) \text{grad div } u - (3\lambda' + 2\mu) \alpha_T \nabla T + F - \rho \ddot{u} = 0,$$

$$\nabla^2 T - \frac{1}{a^2} \frac{\partial T}{\partial t} + \frac{W_0}{\lambda} - \frac{(3\lambda' + 2\mu) \alpha_T T}{\lambda} \text{div } u = 0, \quad (4)$$

where λ' and μ and are the Lamé coefficients [24]; u is the deformation vector; ρ is the density of the material; F is the external force; α_T is the coefficient of

The problem of determining the temperature field was considered in the linear formulation: it was assumed that all thermal and mechanical characteristics of the materials are independent of temperature and energy loss by radiation and convection was neglected. Provided that the characteristic size of the beam is $r_0 < L$, where L is the characteristic size of the irradiated body, and the energy input time is $t < L^2/a^2$, in solving this problem one can use the half-space model. The heating of the sample material is described in this case by the heat conduction equation [22]

$$\frac{\partial T}{\partial t} = a^2 \Delta T \quad (1)$$

at the following initial and boundary conditions:

$$\begin{aligned} \left. \frac{\partial T}{\partial z} \right|_{z=0} &= -\frac{I_0 A_0}{\lambda} f(t) \exp(-K_0 r^2), \\ T(r, z, 0) &= 0, \\ \lim_{r, z \rightarrow \infty} T &< M, \end{aligned} \quad (2)$$

where M is the finite quantity; $f(t)$ is the time function of the laser beam intensity normalised to I_0 ; A_0 is the absorption coefficient of laser radiation on a metal surface; λ is the thermal conductivity of the body material; and T is the temperature.

Using the method of successive integral Hankel and Laplace transforms, we obtain the solution to (1):

ii. *Thermoelastic stresses*

The thermoelastic behaviour of the body is analysed by using the system of equations [22, 23]

thermal expansion; and W_0 is the density of volume heat sources.

In considering the deformation of an elastic metal halfspace whose surface is exposed to pulsed laser radiation, when the inequalities

$$|\rho \ddot{u}| \ll (3\lambda' + 2\mu)\alpha_T |\nabla T|,$$

$$\nabla^2 T \sim \frac{1}{a^2} \frac{\partial T}{\partial t} \gg \frac{(3\lambda' + 2\mu)\alpha_T T}{\lambda} \operatorname{div} u \quad (5)$$

are fulfilled, we can pass to the system of equations of the quasi-stationary thermoelasticity theory:

$$\mu \nabla^2 u + (\lambda' + \mu) \operatorname{grad} \operatorname{div} u - (3\lambda' + 2\mu)\alpha_T \nabla T = 0,$$

$$\nabla^2 T - \frac{1}{a^2} \frac{\partial T}{\partial t} = 0. \quad (6)$$

$$\begin{aligned} \hat{\sigma}_{zz} &= 2GD \int_0^\infty \xi^2 J_0(\xi r) \varphi(\xi) \{e^{-\gamma z} - e^{-\xi z} [1 + z(\xi - \gamma)]\} d\xi, \\ \hat{\sigma}_{rr} &= 2GD \int_0^\infty \varphi(\xi) \left\{ J_0(\xi r) [\xi(\xi z - 2)(\xi - \gamma)e^{-\xi z} + \xi^2 e^{-\xi z} - \gamma^2 e^{-\gamma z}] + \right. \\ &\quad \left. + \frac{J_1(\xi r)}{r} [\xi e^{-\gamma z} - [(\xi - \gamma)(\xi z - 2(1 - \nu)) + \xi] e^{-\xi z}] \right\} d\xi, \\ \hat{\sigma}_{rz} &= 2GD \int_0^\infty \xi \varphi(\xi) J_1(\xi r) [\gamma(e^{-\gamma z} - e^{-\xi z}) - \xi z(\xi - \gamma)e^{-\xi z}] d\xi, \\ \hat{\sigma}_{\varphi\varphi} &= 2GD \int_0^\infty \varphi(\xi) \left\{ J_0(\xi r) [(\xi^2 - \gamma^2)e^{-\gamma z} - 2\nu\xi(\xi - \gamma)e^{-\xi z}] + \right. \\ &\quad \left. + \frac{J_1(\xi r)}{r} \{[(\xi - \gamma)(\xi z - 2(1 - \nu))] + \xi\} e^{-\xi z} - \xi e^{-\gamma z} \right\} d\xi, \end{aligned} \quad (8)$$

where G is the shear modulus; J_1 is the first-order Bessel function;

$$D = \frac{\alpha_T}{2} \frac{1 + \nu}{1 - \nu} \frac{I_0 A a^2}{K_0 \lambda p} \Psi(p); \quad \varphi(\xi) = \frac{\xi}{\gamma} \exp(-\xi^2 / 4K_0);$$

and ν is Poisson's ratio. Analysis of the expression reveals the nature of the time changes at any point in the half-space.

$$W^* = \frac{F_0}{2\pi i} \int_0^\infty d\nu \int_{\sigma-i\infty}^{\sigma+i\infty} dp \frac{\Psi(p/t)}{p} \exp(p - \nu) J_0(\sqrt{\nu} \delta_r) \frac{\sqrt{\nu} - \sqrt{\nu + p/F_0}}{\sqrt{\nu + p/F_0}}, \quad (10)$$

where $F_0 = 4K_0 a^2 \tau$. The resulting expression allows us to trace the changes in the surface shape during irradiation.

Thus, this consideration has made it possible to describe fully the characteristics of temperature fields,

In this case, from the first inequality we obtain the duration of a single pulse

$$\tau \gg \max\left(\frac{\rho a^2}{\lambda'}, \frac{\rho a^2}{\mu}\right) \sim 10^{-6} - 10^{-8} \text{ s}, \quad (7a)$$

and from the second –

$$\tau^{3/2} \ll \frac{\rho^2 c^2 a}{\mu \alpha_T I_0 A}. \quad (7b)$$

We represented the stress tensor components in the general form [21]:

iii. Thermal deformations

The stress state occurring in a solid body is accompanied by its deformation, its largest amplitude being achieved on the irradiated surface. The expression for the normal displacement of the surface, corresponding to a given temperature distribution, has the form:

$$W(r, z, t) = W^* \frac{(1 + \nu)\alpha_T I_0 A}{\lambda K_0}, \quad (9)$$

thermoelastic stresses and thermal deformations occurring in solids whose surface is exposed to high-power laser radiation varying with time in an arbitrary manner. In addition, the following relations are fulfilled between the quantities characterising the thermal stress state in the

continuous-wave and any other nonstationary regime of energy input into the solid [22, 24]:

$$\begin{aligned}
 T^{tr} &= \int_0^t f(t-\tau) \frac{\partial T^{st}}{\partial \tau} d\tau, \\
 \sigma_{ik}^{tr} &= \int_0^t f(t-\tau) \frac{\partial \sigma_{ik}^{st}}{\partial \tau} d\tau, \\
 W^{tr} &= \int_0^t f(t-\tau) \frac{\partial W^{st}}{\partial \tau} d\tau.
 \end{aligned}
 \tag{11}$$

deformation component of the POE as a whole can be reduced to zero due to the large thickness of its effectively cooled base. Later, both components of the POE deformation were examined in the book of L.S. Tsesnek et al. [25].

b) Continuous-wave irradiation

i. Temperature field

If the time of laser irradiation satisfies the inequality $r_0^2/a^2 \leq t \leq L^2/a^2$, a steady-state temperature field can be established in the sample material. The main property of the process of its establishment is described by the expression [21]

$$T^* = \frac{2}{\sqrt{\pi}} \arctan \sqrt{F_0}. \tag{12}$$

It follows from (12) that for instants of times t , at which $F_0 \geq 4$, the current temperature is 10% less than the steady-state value. We therefore assume that, starting at time t , at which $F_0 > 4$, a stationary thermal state is established in the sample material (Fig. 3.7.1).

The expression for the temperature field in the half-space has the form [21]

$$T^* = \int_0^\infty J_0(\sqrt{\nu} \delta_r) \exp[-\sqrt{\nu}(\delta_z + \sqrt{\nu})] \frac{d\nu}{\sqrt{\nu}}, \tag{13}$$

where $\delta_z = 2\sqrt{K_0}z$ and $\delta_r = 2\sqrt{K_0}r$. From this expression we obtain the locality of the temperature field, the characteristic values of which decrease with increasing distance from the centre of the surface irradiation region and inside the material (Figs. 3.7.2–3.7.4).

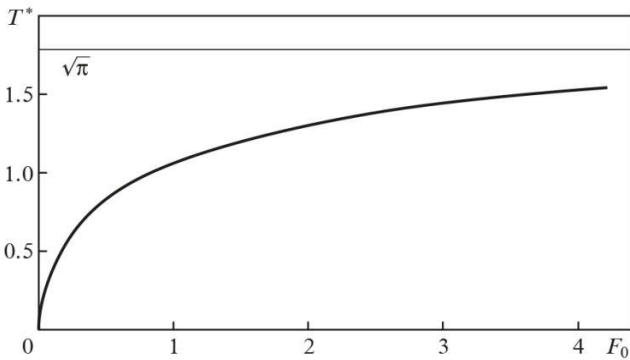


Figure 3.7.1: Time dependence of the sample surface temperature at the centre of the region (number F_0) exposed to cw radiation

These relations are similar to Duhamel's integral formula from the theory of heat conduction. It should be noted that the local deformation of the POE surface is the determining factor of the laser impact and the bending

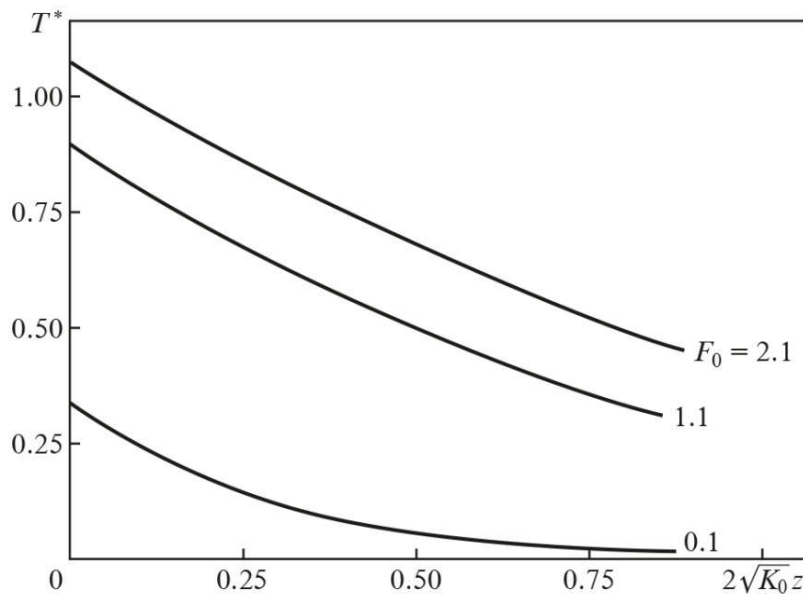


Figure 3.7.2: Temperature field distribution on the z axis

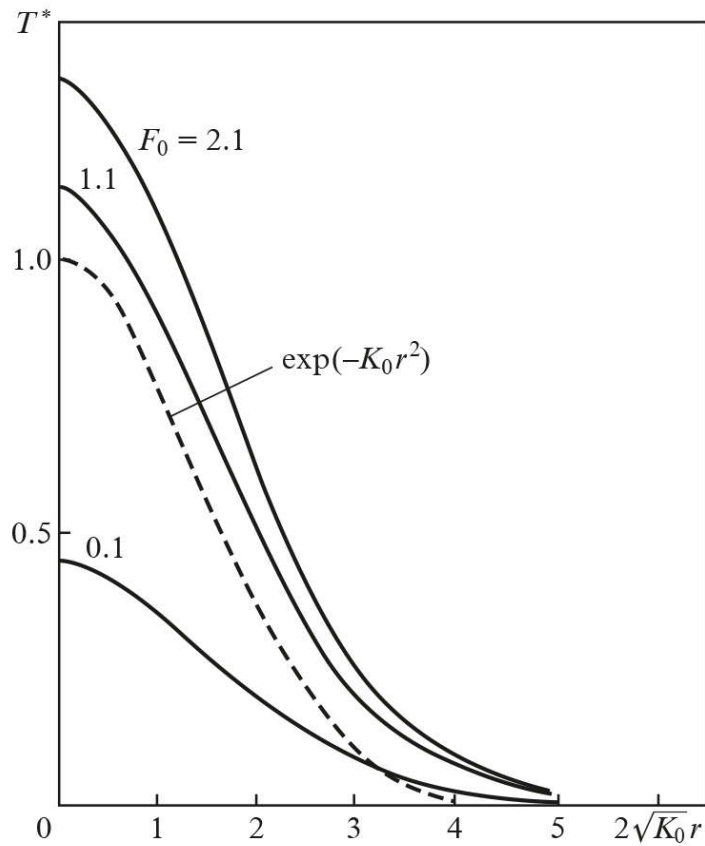


Figure 3.7.3: Temperature field distribution on the sample surface

ii. Thermoelastic stresses

In the steady-state regime ($p \rightarrow 0$), nonzero are only the components of the tensor of thermal stresses σ_{rr}^* and $\sigma_{\varphi\varphi}^*$ [21]:

$$\sigma_{rr}^* = 2(1-\nu) \int_0^\infty \exp[-\sqrt{\nu}(\sqrt{\nu} + \delta_z)] [J_1(\sqrt{\nu}\delta_r) - J_0(\sqrt{\nu}\delta_r)] \frac{d\nu}{\sqrt{\nu}}, \tag{14}$$

$$\sigma_{\varphi\varphi}^* = 2(1-\nu) \int_0^\infty \exp[-\sqrt{\nu}(\sqrt{\nu} + \delta_z)] [-J_1(\sqrt{\nu}\delta_r) / (\nu\delta_r)] d\nu,$$

where

$$\sigma_{ik}^* = \frac{\lambda\sqrt{K_0}(1-\nu)}{I_0AG\alpha_T(1+\nu)} \sigma_{ik}(r).$$

The maximum values of these components are achieved in the centre of the irradiated region (Fig. 3.7.5) on the surface of the half-space, where the stationary field of thermoelastic stresses have the form (Figs. 3.7.6 and 3.7.7)

$$\begin{aligned} \sigma_{rr}^* &= \frac{\sqrt{\pi}(1-\nu)}{2} {}_1F_1\left(\frac{1}{2}; 2; -\delta_r^2/4\right), \\ \sigma_{\varphi\varphi}^* &= \frac{\sqrt{\pi}(1-\nu)}{2} \left[{}_1F_1\left(\frac{1}{2}; 2; -\delta_r^2/4\right) - {}_1F_1\left(\frac{1}{2}; 1; -\delta_r^2/4\right) \right]. \end{aligned} \tag{15}$$

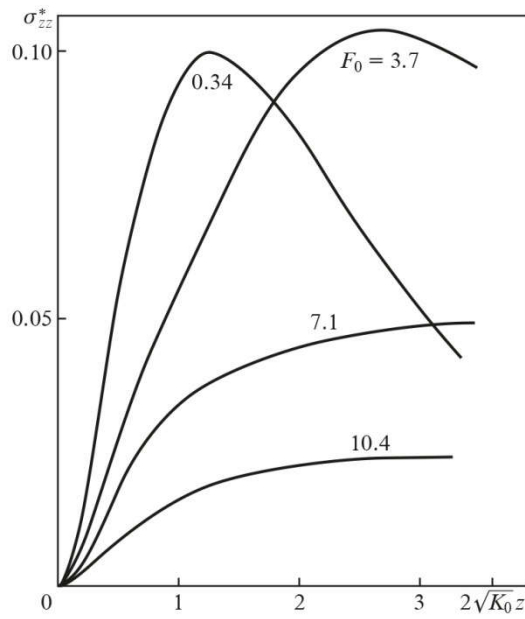


Figure 3.7.4: Dependence of the axial stress σ_{zz} on the exposure time of laser irradiation

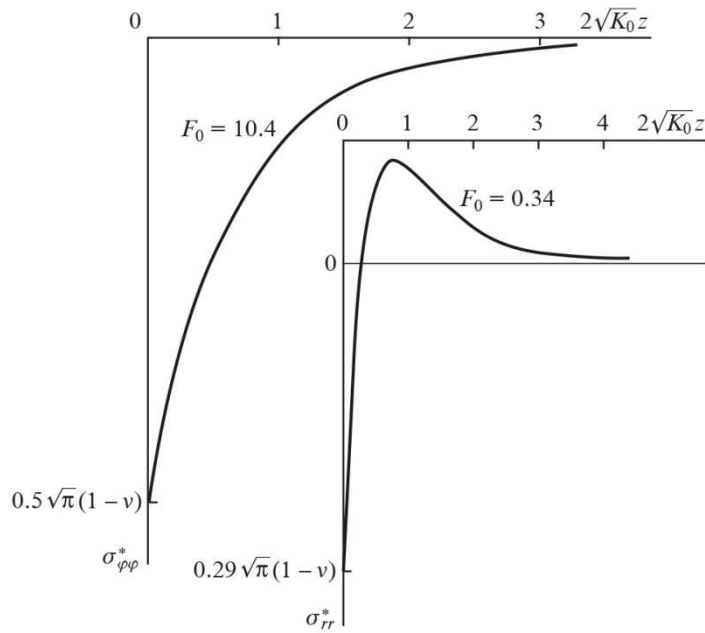


Figure 3.7.5: Distribution of the peripheral ($\sigma_{\varphi\varphi}$) and radial (σ_{rr}) tensor components on the z axis for different exposure times of laser irradiation

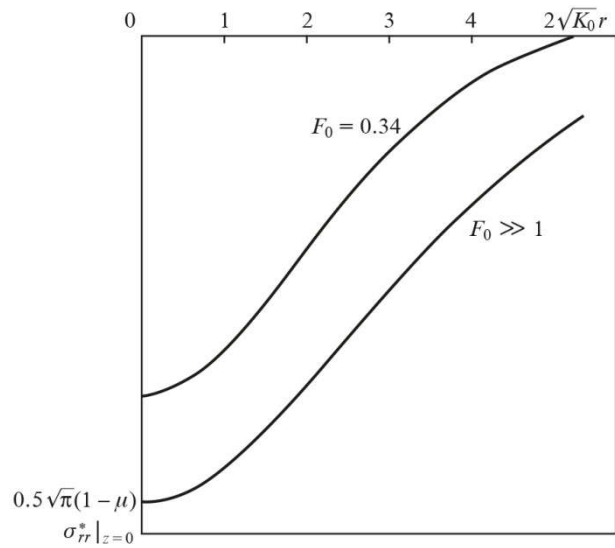


Figure 3.7.6: Stress field σ_{rr} on the surface of the half-space

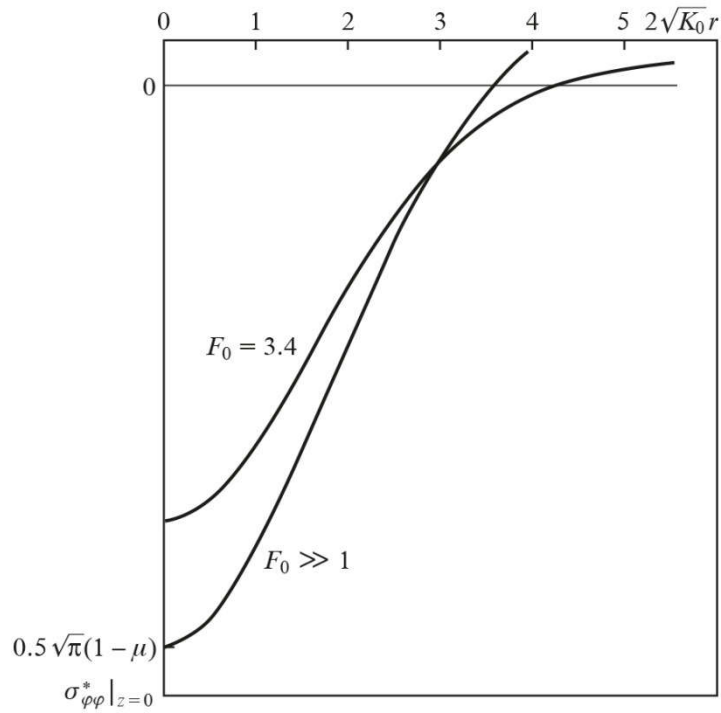


Figure 3.7.7: Stress field $\sigma_{\varphi\varphi}$ on the surface of the half-space



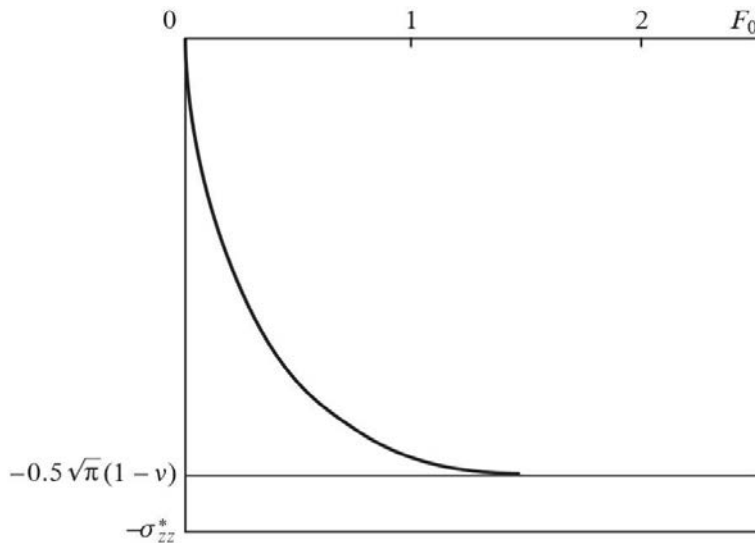


Figure 3.7.8: Establishment of a stationary stress state on the surface, in the centre of the irradiated region

The main property in establishing a steady state for σ_{rr} and $\sigma_{\varphi\varphi}$ are characterised by the dependence shown in Fig. 3.7.8:

$$\sigma_{ii}^*(\delta_r = \delta_z = 0) = \frac{1+\nu}{\sqrt{\pi}} \left[F_0 \left(\arctan \frac{1}{\sqrt{F_0}} - \frac{1}{\sqrt{F_0}} \right) - \frac{1-\nu}{1+\nu} \arctan \sqrt{F_0} \right]. \quad (16)$$

This expression completely describes the characteristics of the stressed state arising in a solid when its surface is irradiated by cw laser radiation.

iii. Thermal deformation of the surface

The expression for the displacement W^* of the reflective surface in the half-space model has the form [21]:

$$W^* = -\frac{1}{2} \left\{ F_0 \exp(-\delta_r^2/4) - \left[\frac{4\sqrt{F_0}}{1+F_0} - 2 \ln(\sqrt{F_0} + \sqrt{F_0+1}) \right] {}_1F_1 \left(\frac{3}{2}; 1; -\frac{\delta_r^2}{4} \right) \right\}. \quad (17)$$

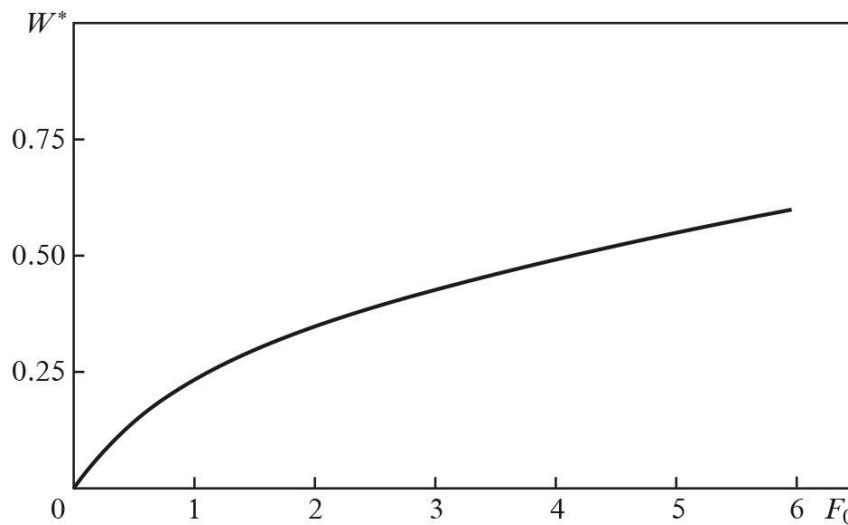


Figure 3.7.9: Establishment of a quasi-stationary deformation state on the surface, in the centre of the irradiated region

Deformation surface profiles for different exposure times are shown in Fig. 3.7.9.

c) Pulsed irradiation

i. Temperature field

In the case of short irradiation times, the depth of the temperature field penetration into the material is

$$T^* = \frac{2}{\sqrt{\pi}} [\Theta(t^*) \arctan(\sqrt{F_0 t^*}) - \Theta(t^* - 1) \arctan(\sqrt{F_0(t^* - 1)})] \exp(-K_0 r^2), \tag{18}$$

where $\Theta(t^*)$ is the Heaviside function; $t^* = t / \tau$; and τ is the pulse duration.

ii. Thermoelastic stresses

Thermoelastic stresses arising in a solid irradiated by laser light play an important role in the destruction of the optical surface of the POE. Under pulsed irradiation ($F_0 \ll 1$) the expressions for the

$$\begin{aligned} \sigma_{rr}^*(\delta_r = 0) &= -\frac{2}{\sqrt{\pi}} \sqrt{F_0} \left[\exp(-\delta_z^2 / 4F_0) - \frac{\sqrt{\pi} \delta_z}{2F_0} \operatorname{erfc}\left(\frac{\delta_z}{2\sqrt{F_0}}\right) \right] \approx \\ &\approx \frac{8F_0^{3/2}}{\sqrt{\pi} \delta_z^2} \exp\left(-\frac{\delta_z^2}{4F_0}\right), \end{aligned} \tag{19}$$

where

$$\frac{\delta_z}{2\sqrt{F_0}} \gg 1.$$

The maximum values of the components σ_{rr}^* and $\sigma_{\varphi\varphi}^*$ are achieved on the surface,

$$\sigma_{rr}^* = \sigma_{\varphi\varphi}^* = -2\sqrt{F_0 / \pi} \exp(-\delta_r^2 / 4), \tag{20}$$

i.e., the distribution of the components σ_{rr}^* and $\sigma_{\varphi\varphi}^*$ on the surface repeat the laser beam intensity distribution.

$$\sigma_{rz}^* = -\frac{\delta_r}{2} \exp\left(-\frac{\delta_r^2}{4}\right) \left[F_0 t^* \operatorname{erf}\left(\frac{\delta_z}{2\sqrt{F_0 t^*}}\right) + \frac{\sqrt{F_0 t^*}}{\pi} \delta_z \exp\left(-\frac{\delta_z^2}{4F_0 t^*}\right) \right], \tag{22}$$

where V is a transform variable. The difference in signs of the components means that in the case of thermal deformation of the sample by laser radiation, for σ_{zz} tension of a material is realised, whereas for σ_{rz} – compression. The maximum value of σ_{zz}^* is achieved on the z axis; in this case, $\delta_z^{\max} \approx \sqrt[4]{12}$, i.e., $z_0^{\max} \approx 0.66r_0$, and $\sigma_{zz}^{\max} \approx 1.9F_0$. The component σ_{rz}^* reaches its maximum value at point $r_0^{\max} = r_0 / 2$ and $z_0^{\max} \approx 2\sqrt{a^2 t}$:

proportional to $\sqrt{a^2 t} \ll r_0$; therefore, the radial heat spreading can be ignored, and the temperature distribution over the surface repeats the laser beam intensity distribution profile [26]:

stress tensor components are given by (15), because in this case the propagation of heat in a solid is of quasi-one-dimensional character and the radial heat spreading can be neglected. The depth of penetration of thermal stresses in the material is $\sqrt{a^2 \tau} \ll r_0$, which follows from the form of σ_{ik} on the z axis:

The components σ_{rr}^* and $\sigma_{\varphi\varphi}^*$ on the surface $z = 0$ are equal, and the expression for $\sigma_{ii}^*(\delta_r, \delta_z = 0)$ has the form:

$$\sigma_{ii}^* = -\frac{2}{\sqrt{\pi}} [\Theta(t^*) \sqrt{F_0 t^*} - \Theta(t^* - 1) \sqrt{F_0(t^* - 1)}]. \tag{21}$$

In the case of small irradiation times

$$\sigma_{zz}^* = 2\delta_z F_0 t^* \int_0^\infty V^3 \exp(-V^2 - V\delta_z) dV,$$

$$\sigma_{rz}^{\max} \approx -0.5F_0. \tag{23}$$

A distinctive feature of the behaviour of the σ_{zz}^* component is that if the inequality $F_0 \ll 1$ is fulfilled, the position of its maximum on the z axis is determined by the spatial characteristics of the laser beam rather

than the irradiation time. The maximum of this component is achieved by the end of the laser pulse. This feature is explained by the fact that at $F_0 t^* \ll 1$ the region of thermoelastic perturbations lies on the sample surface and localises in the irradiation region, because heat due to heat conduction has no time to spread over the sample material. In the opposite case, i.e., at $F_0 t^* > 1$, the point of this component maximum is determined from the condition $\delta z^2 / (4F_0 t^*) = 1$.

iii. *Thermal deformations*

The expression for the thermal deformation of the reflecting surface irradiated by a rectangular laser pulse, whose duration satisfies the condition $F_0 \ll 1$, has the form [21]:

$$W^* = -\frac{F_0}{2} \exp(-K_0 r^2) [\Theta(t^*) t^* - \Theta(t^* - 1)(t^* - 1)]. \quad (24)$$

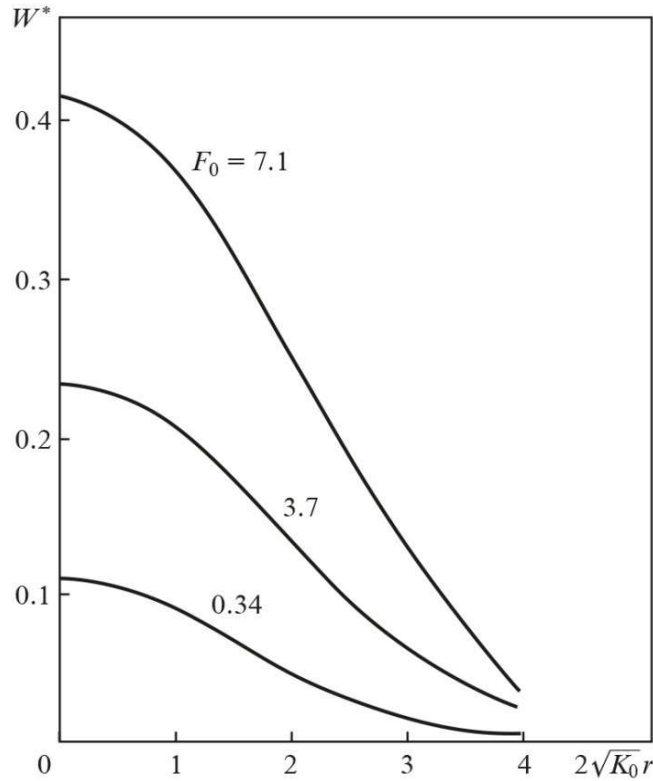


Figure 3.7.10: Deformation surface profiles for different exposure times

The distribution of thermal deformations of the reflecting surface repeats the laser beam intensity distribution (Fig. 3.7.10), which we used in our method of the dynamic control of the intensity distribution of laser radiation [27].

d) *Repetitively pulsed irradiation*

Thermal deformations of a solid body exposed to repetitively pulsed laser radiation were analysed by using the previously derived relations that are similar to Duhamel's integral formulas. The energy flow was treated as a train of rectangular pulses having a duration r , period T_0 (repetition rate $\nu_0 = 1/T_0$) and off-duty ratio $SQV = \tau/T_0$. It was assumed that $F_0 = 4K_0 a^2 T_0 < 1$. The arising thermal stresses and deformations of the temperature field are expressed in terms of the integrals (typical of the cw regime) that are similar to Duhamel's integrals [28]:

$$F^{PP} = \int_0^t f(t - \tau) \frac{\partial F^{cw}}{\partial \tau} d\tau. \quad (25)$$

At the initial instants of time, i.e., when $F_0 t^* < 1$, repetitively pulsed irradiation is similar to pulsed irradiation. The geometric meaning of (25) is characterised by the area of the integrals in Fig. 3.7.11. (For the temperature and the components $\sigma_{\varphi\varphi}$ and σ_{rr} , the value of $\partial F^{cw} / \partial \tau$ tends to infinity as $1/\sqrt{t}$ at $t \rightarrow 0$ and to zero at $t \rightarrow \infty$; for deformation $\partial F^{cw} / \partial \tau$ tends to const at $t \rightarrow 0$ and to zero at $t \rightarrow \infty$.) In the case of long irradiation times, i.e., when $F_0 t^* > 1$, the temperature and thermal stresses reach their quasi-steady states, i.e., a constant component of these values becomes similar to that in the cw regime of energy input with a reduced intensity $I_0 SQV$. In this case,

against the background of this component, along with changes in the laser beam intensity, there will be the characteristic peaks of temperature and stress, which are similar to peaks during pulsed irradiation. A separate

'pulse' of thermal deformations of the reflecting surface exists against the background of a 'stationary component' tending to infinity.

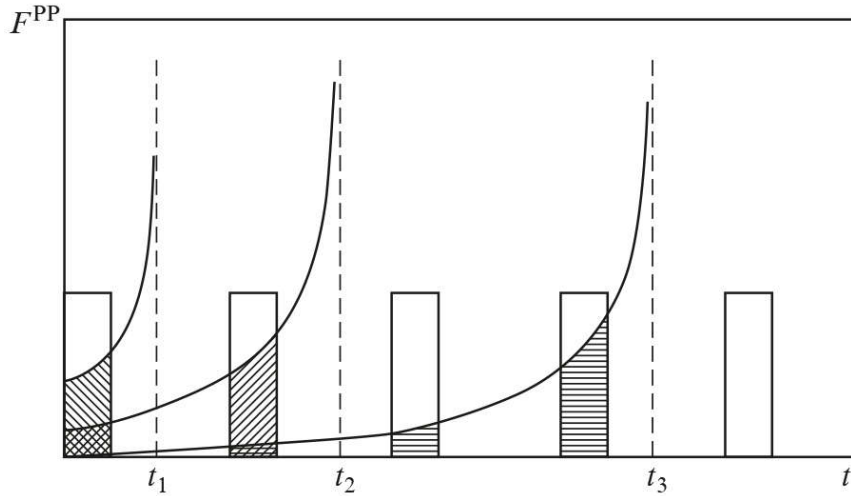


Figure 3.7.11: Geometrical interpretation of Duhamel's integrals

i. Temperature field

The expression for the temperature has the form [21]

$$T^* = \frac{1}{2\pi i} \int_{\sigma_i - i\infty}^{\sigma_i + i\infty} dp \Psi(p) e^{p t} \int_0^\infty \frac{e^{-V} J_0(\sqrt{V} \delta_r) \exp[-\sqrt{V}(\sqrt{V} + \delta_z)]}{\sqrt{8/F_0 + V}} dV, \quad (26)$$

since for a train of pulses

$$\Psi(p) = \frac{[1 - \exp(-p\tau)] \{1 - \exp[-p(N+1)T]\}}{p[1 - \exp(-pT)]} \quad (27)$$

is the Laplace transform of $f(t)$; and N is the number of propagated laser pulses.

In the centre of the irradiation region the temperature reaches a maximum value by the time the next pulse terminates ($F_0 > 1$):

$$T_{\max}^* = \sqrt{\pi} \text{SQV} + \frac{2}{\sqrt{\pi}} \arctan \sqrt{F_0 \text{SQV}}, \quad (28)$$

where SQV is the off-duty ratio of the temporal structure of radiation.

ii. Thermoelastic stresses

Maximum values of the radial and circumferential tangential stress are achieved in the centre of the irradiation region, where they are equal to each other:

$$\sigma_{ii}^{PP} = \int_0^t f(t-\tau) \frac{\partial \sigma_{ii}^{cw}}{\partial \tau} d\tau \quad (29)$$

[σ_{ii}^{cw} is determined from (16)]. The field distribution of stresses σ_{ii}^* on the surface by the time when the next laser pulse terminates has the form:

$$\sigma_{ii}^* = \text{SQV} \sigma_{ii}^{*(1)} + \sum_{n=0}^N \Theta(n+1-t^*) [\Theta(t^*-n) \times \sigma_{ii}^{*(2)}(t^*-n) - \Theta(t^*-n-\text{SQV}) \sigma_{ii}^{*(2)}(t^*-n-\text{SQV})], \quad (30)$$

where $\sigma_{\varphi\varphi}^{*(1)}$ and $\sigma_{rr}^{*(1)}$ are determined from (16), and $\sigma_{\varphi\varphi}^{*(2)} = \sigma_{rr}^{*(2)}$ - from (21). Because in the steady stress state σ_{zz} and σ_{rz} are identically zero, their values in the case of repetitively pulsed irradiation are the same as in the case of pulsed irradiation (accuracy \sim SQV).

iv. Deformation of the surface

The displacement of a solid-body surface exposed to repetitively pulsed radiation also has stationary and pulse components [21]:

$$W^* = \text{SQV} W^{*(1)} + W^{*(2)}$$

When the quasi-stationary state is reached

$$W^* = -\text{SQV} \ln 2 \sqrt{F_0} F1 \left(\frac{3}{2}; 1; -\frac{\delta_r^2}{\pi} \right) - \frac{F_0}{2} \sum_{n=0}^N \Theta(n+1-t^*) [\Theta(t^*-n)(t^*-n) - \Theta(t^*-n-\text{SQV})(t^*-n-\text{SQV})] \exp(-K_0 r^2). \quad (31)$$

e) *Criteria for the optical surface stability*

Expressions given for the characteristics of the thermal stress state of a solid whose surface is irradiated by high-power cw, pulsed and repetitively pulsed laser radiation allowed us to determine the limiting intensities corresponding to different stages of the optical damage of mirror surfaces [21, 29]. To this end, the parameters of the optical surface stability include not only the thermophysical and mechanical properties of the material but also the parameters of a Gaussian-like beam, namely the intensity in the centre of the irradiation region, the size of the irradiation region and the duration of a single pulse and, in the case of repetitively pulsed irradiation, – the pulse train off-duty ratio. The stability parameters of the reflector contain the ratio of a maximum value of the thermal stress state characteristic to its value at which the solid material experiences irreversible macroscopic changes – melting, plastic (brittle) or fatigue deformation or achievement of a critical value $\lambda_0/20$ by the amplitude of thermal deformation of the optical surface, where λ_0 is the wavelength of the laser used. The thus introduced stability parameters of mirrored POE surfaces made it possible not only to compare different pure metals and their alloys in terms of applicability in power optics but also to create specific types of combined POEs capable of withstanding high-power fluxes of cw, pulsed and repetitively pulsed laser radiation.

i. *Continuous-wave regime*

A solid body whose surface is exposed to cw laser radiation is destroyed when the temperature field in the centre of the irradiation region reaches the melting point of the material and the components of the stress field reach the yield point. The stability of the optical surface under cw irradiation is characterized by the parameters

$$\gamma_{T_{\text{melt}}}^{\text{cw}} = \frac{\sqrt{\pi} I_0 A}{2\lambda \sqrt{K_0} T_{\text{melt}}}, \quad \gamma_{\sigma_T}^{\text{cw}} = \frac{\sqrt{3\pi} (1+\nu) I_0 A G \alpha_T}{2\lambda \sqrt{K_0} \sigma_T} \quad (32)$$

If $\gamma_{T_{\text{melt}}}$ and $\gamma_{\sigma_T} < 1$, the material will undergo no irreversible changes. The values of these parameters in the case of cw laser radiation at a power density $I_0 A = 1 \text{ kW cm}^{-2}$ and $K_0 = 8 \times 10^2 \text{ m}^{-2}$ are shown in Table 3.7.1 for Cu, Al and Mo. The main reason for the damage of the optical surface can be determined from the relation

$$\gamma_{\text{rel}}^{\text{cw}} = \frac{\gamma_{\sigma_T}^{\text{cw}}}{\gamma_{T_{\text{melt}}}^{\text{cw}}} = \frac{\sqrt{3}(1+\nu) G \alpha_T T_{\text{melt}}}{\sigma_T}. \quad (33)$$

If $\sigma_{\text{rel}}^{\text{cw}} > 1$, the material will be destroyed when the component σ_{ii} reaches the yield point, or when the melting point of the material, $T(0,0,\infty)$ is reached.

For the materials in question (Table 3.7.1), the main reason for the deterioration of the optical surface at lower laser intensities is irreversible plastic deformations of the POE in the centre of the irradiation region. There is another important reason for the deterioration of the optical surface – excess of the critical value $\lambda_0/20$ by the value of thermal deformation of the optical surface – which is implemented at long exposure times of high power laser radiation and in the range of the parameters corresponding to the elastic deformation of the material. In this case, phase and energy characteristics of the reflected laser beam are markedly impaired. The criterion for the optical surface stability to such changes in the optical characteristics of the reflector is given by parameter

$$\gamma_{\lambda_0/20}^{\text{cw}} = \frac{20(1+\nu)\alpha_T I_0 A}{\lambda K_0 \lambda_0} \ln 2 \sqrt{F_0}. \quad (34)$$

The value $\gamma_{\lambda_0/20}^{\text{cw}} < 1$ can be reached if use is made of some types of reflector designs with efficient cooling [30].

Table 3.7.1: Parameters of stability and threshold intensities for Al, Mo and Cu at $I_0A = 1 \text{ kW cm}^{-2}$, $r_0 = 5 \text{ cm}$, and $t = 5 \times 10^{-5} \text{ s}$

Parameter	Cu	Material Mo	Al
CW regime			
$\gamma_{T_{\text{melt}}} = \frac{\sqrt{\pi} I_0 A}{2\lambda\sqrt{K_0}} \frac{1}{T_{\text{melt}}}$	0.74	0.8	2.3
$I_{\text{th}} = \frac{1}{\gamma_{T_{\text{melt}}}} / \text{kW cm}^{-2}$	1.4	1.3	0.44
$\gamma_{\sigma_T} = \frac{\sqrt{3\pi} I_0 A G \alpha_T (1+\nu)}{2\lambda\sqrt{K_0} \sigma_T}$	19.3	10^4	38.3
$I_{\text{th}} = \frac{1}{\gamma_{\sigma_T}} / \text{kW cm}^{-2}$	0.05	10^{-4}	2.6×10^{-2}
Pulsed regime			
$\gamma_{T_{\text{melt}}} = \frac{\sqrt{\pi} I_0 A}{2\lambda\sqrt{K_0}} \frac{1}{T_{\text{melt}}}$	2.0×10^{-3}	1.45×10^{-3}	5.4×10^{-3}
$I_{\text{th}} = \frac{1}{\gamma_{T_{\text{melt}}}} / \text{kW cm}^{-2}$	500	700	190
$\gamma_{\sigma_T} = \frac{\sqrt{3\pi} I_0 A G \alpha_T (1+\nu)}{2\lambda\sqrt{K_0} \sigma_T}$	0.16	55	0.28
$I_{\text{th}} = \frac{1}{\gamma_{\sigma_T}} / \text{kW cm}^{-2}$	6.3	1.8×10^{-2}	3.6

ii. Pulsed regime

The parameters of the optical surface stability under pulsed irradiation by a Gaussian-like laser beam having a duration τ and intensity I_0 in the centre of the irradiation region, determined by the ability to reach critical values T_{melt} , σ_T and $\lambda_0/20$ by temperature $T(0,0,\tau)$, thermoelastic stresses $\sigma_{ii}(0,0,\tau)$ and thermal deformations $W(0,0,\tau)$, have the form [29]:

$$\gamma_{T_{\text{melt}}}^P = \frac{2I_0A}{\sqrt{\pi}\lambda T_{\text{melt}}} \sqrt{a^2\tau},$$

$$\gamma_{\sigma_T}^P = 4\sqrt{\frac{3}{\pi}} \frac{I_0AG\alpha_T(1+\nu)}{\lambda G_T(1-\nu)} \sqrt{a^2\tau}, \quad (35)$$

$$\gamma_{\lambda_0/20}^P = \frac{40(1+\nu)I_0A\alpha_T a^2\tau}{\lambda\lambda_0}.$$

The values of these parameters, found for copper, aluminium and molybdenum at $I_0A = 1 \text{ kW cm}^{-2}$, $K_0 = 2.82 \times 10^2 \text{ m}^{-2}$ and $\tau = 50 \text{ }\mu\text{s}$, and the heat flow values I_0A , at which $\gamma_i^P = 1$, are presented in Table 1. In the cw regime, the optical surface properties are mainly degraded due to irreversible plastic deformations in the centre of the irradiation region. Under pulsed irradiation

the behaviour of the thermal stress state is more complicated than under cw irradiation. Thus, in contrast to the stationary thermal stress state, the nonstationary state in the material of a solid is characterised by the presence of the nonzero components σ_{zz} and σ_{rz} . In this case, the highest value is reached by the component σ_{zz} on the z axis at a distance of $\sim 0.66r_0$ from the optical surface. If at some level of these I_0A values the component σ_{zz} is greater than the strength modulus σ_b , it is possible to implement the conditions of brittle fracture, at which the surface layer of the POE material will be detached. For this type of destruction the parameter of the optical surface stability has the form:

$$\gamma_{\sigma_b}^P = \frac{4I_0AE\alpha_T a^2\tau\sqrt{K_0}}{(1-\nu)\lambda\sigma_b},$$

and the stability parameter defined with respect to plastic deformation, has the form:

$$\gamma_{\sigma_T}^P = \frac{\sqrt{3}I_0AE\alpha_T F_0}{\lambda\sqrt{K_0}(1-\nu)\sigma_T} \left[1 + 2\frac{\sqrt{F_0}}{3\pi} \exp\left(-\frac{\sqrt{3}}{2F_0}\right) \right], \quad (36)$$

The values of the parameters and their corresponding intensities for Al, Mo and Cu are listed in Table 3.7.1.

iii. *Repetitively pulsed regime*

The state of a solid body, whose surface is irradiated by repetitively pulsed laser pulses, combines the characteristic features of thermal stress states under pulsed and cw irradiation. In this case, for the temperature fields, the fields of the components σ_{rr} and $\sigma_{\varphi\varphi}$, the stress tensor and the thermal deformation fields the realisable temperature and thermal stress states are a combination of stationary and nonstationary states. In this regard, the stability parameters of the reflecting surfaces, defined by the ability of the temperature to reach the melting point of the material, of the components σ_{rr} and $\sigma_{\varphi\varphi}$ to reach the yield point and of thermal deformation to reach the threshold $\lambda_0/20$, are as follows [21]:

$$\gamma_i^{PP} = \text{SQV} \gamma_i^{cw} + \gamma_i^P. \quad (37)$$

Under repetitively pulsed irradiation, a nonstationary, cyclically repeated stress state arises on a solid surface in the material. As a result, the material of the solid body may experience irreversible fatigue damage. The conditions under which the POE surface undergoes macroscopic fatigue fracture can be assessed by Wohler curves, determining the dependence of modulus of the amplitude of fatigue stresses on the number of cycles of the loading pulses N_p [21, 31].

f) *Irreversible changes in the optical surface*

Dynamics of the fatigue and brittle fracture is characterised by the emergence and extension of microcracks. Therefore, inadmissibility of destruction of the optical POE surface is dictated by the need to preserve the diffusely scattered component of laser radiation at negligible levels. Moreover, the origin and development of microcracks is accompanied by microstructural and phase transformations of the material, leading to a change in the structural and phase composition of the reflecting surface and, as a consequence – to an increase in its absorption coefficient A , whereas the adsorption of various substances on the resulting system of microcracks initiating an optical breakdown leads to a decrease in radiation resistance of the reflecting surface. Furthermore, the optical breakdown of air near the target can occur without the segregation of impurities directly in the vicinity of emergence of microcracks, because they become the nucleus of the electric fields, etc. We considered sequentially the basic mechanisms of microstructural and phase transformations preceding the stage of plastic, fatigue and brittle fracture or accompanying these stages, as well as analysed the possible reasons for the change in the optical surface quality. The expressions obtained are important not only for the problems of power optics. They are effectively used today for the analysis of the conditions of fracture of solids of different nature due to excess of limiting

stresses for the various components of the stress tensor.

III. STATIC OPES BASED ON MATERIALS WITH A POROUS STRUCTURE

The feasibility of using porous structures for cooling thermally stressed POEs was justified theoretically and experimentally in our papers [32–39]. An increase in the optical damage threshold of laser reflectors based on porous structures was provided by a 'minimum' thickness of the separating layer (tens of microns), by the heat transfer intensification, by high permeability of the heat exchanger for the selected coolants pumped through the porous structure and by the use of the heat exchanger with a significantly developed surface. The test results of water-cooled POEs that are based on the porous structures indicated the possibility of removal of high heat flows at low values of the mirror surface deformations. The maximum density of the heat flow being removed, which does not lead to destruction of the mirror surface, was equal to 8.2 kW cm^{-2} . At $q = 2 \text{ kW cm}^{-2}$ the value of thermal deformation was $\sim \lambda_0/20$, where $\lambda = 10.6 \text{ }\mu\text{m}$ [32, 33].

A further increase in the optical damage threshold of cooled mirror surfaces can be realized by the optimization of the porous structure parameters [34, 38, 39], the appropriate choice of the coolant [21], the development of the technology of fabrication of a thin separating layer based on intermetallic compounds [32] and the rational design of the POE on the whole [35–37]. The development of a cooled POE requires a detailed study of heat and mass transfer in porous structures. These processes at the beginning of research in the field of high power/energy optics were either insufficiently studied or not studied at all.

a) *Temperature field in porous structures under convective cooling*

The temperature fields in porous structures are calculated in the one-dimensional formulation under the following assumptions: the incident radiation is uniformly distributed over the irradiated surface; the thickness of the porous layer Δ_p is much greater than the depth of heating, which makes it infinitely large ($\Delta_p \rightarrow \infty$) and allows consideration of the half-space model; and the temperature and velocity of the flow through the thickness the porous layer are constant. The heat transfer equation, which describes the temperature distribution over the thickness of the porous layer, can be written in the dimensionless form:

$$\frac{d^2\Theta}{d\bar{x}^2} = N(\Theta - 1), \quad (38)$$

where $\Theta = t/t_T$, $\bar{x} = x/d_m$ and $N = \tilde{Nu}N'$ are the dimensionless temperature, coordinate and Nusselt number, respectively; d_m is the mean diameter of the structure particles; $\tilde{Nu} = h_m d_m / \tilde{\lambda}$ is the modified Nusselt number, which characterises the ratio of the convective cooling to the heat transfer due to skeleton thermal conductivity; $N' = S_v d_m$ is a dimensionless parameter; and S_v is the heat transfer surface.

The boundary conditions of this equation can be written in the form:

$$\bar{x} = 0, \quad d\Theta/d\bar{x} = -\tilde{Nu}\bar{q}\bar{x} \rightarrow \infty, \quad \Theta \rightarrow 1, \quad (39)$$

where $\bar{q} = q/(h_m t_T)$ is the dimensionless heat flux density and q is the heat flux density transmitted through the separating layer. The solution to this equation has the form [21, 34]

$$\Theta(\bar{x}) = 1 + \bar{q} \sqrt{\tilde{Nu}/N'} \exp(-\sqrt{N}\bar{x}). \quad (40)$$

It follows from (40) that the rate of temperature decrease over the thickness of the porous structure is determined by the parameter \sqrt{N} . The maximum heat flux density, removed from the reflector due to convective cooling, follows from the condition of equality of the coolant temperature Θ_p at a fixed pressure to the boiling temperature Θ_{boil} of the coolant ($\Theta_p = \Theta_{boil}$) at a chosen pressure and has the form:

$$\bar{q}_{max} = (\Theta_{boil} - 1) \sqrt{N'/\tilde{Nu}}. \quad (41)$$

The degree of heat transfer intensification in a porous structure as a result of the turbulent flow circulation and the surface development is determined by the coefficient K_{int} , which characterises the ratio of the amount of heat removed by the coolant in the structure under consideration to the amount of heat that would be removed directly from the cooling surface of the separating layer by the coolant when it flows in a slot gap of depth Δ [40]:

$$K_{int} = q/h_\Delta(t_{\bar{x}=0} - t_T), \quad (42)$$

where h_Δ is the coefficient of convective heat transfer in the coolant flow in a slot gap. For example, for the turbulent regime of the coolant flow the Nusselt number has the form

$$Nu_\Delta = 0.023 Re^{0.8} Pr^{0.4}, \quad (43)$$

where Re and Pr are the Reynolds and Prandtl numbers.

In the case of removal of heat fluxes, the depth of heating is [41]

$$\bar{\Delta}_{max} = N^{-1/2} \ln 10^2 (\Theta_{boil} - 1). \quad (44)$$

In combination with the expressions describing the flow hydrodynamics, the obtained dependences are the basis for optimising the parameters of porous structures, ensuring minimal thermal deformations of POE surfaces or, if necessary, the maximum heat fluxes, removed in the case of convective cooling.

b) Convective heat transfer in a porous structure

The regime of the coolant flow in porous materials, which is of interest for high-power optics, is a transition between laminar and turbulent regimes. The criterion equation of the interporous convective heat transfer for gases and droplets can be represented in the form [41]

$$Nu = c(RePr)^n, \quad (45)$$

where c and n are the constants depending only on the structural characteristics of the porous material.

Using known experimental data from the literature [42], we analysed the dependences of c and n on the structural characteristics of porous structures for which these constants are quite authentically known. As a result, we found that c and n depend mainly on the bulk porosity Π_v . Thus, relation (45) for the dimensionless Nusselt number with account for correlation expressions $c(\Pi_v)$ and $n(\Pi_v)$ allows one to calculate the coefficient of convective heat transfer in porous structures.

c) Hydrodynamics of a single-phase flow in a porous structure

The temperature field and thermal deformation of the POE are largely determined by the flow rate of the coolant pumped through a porous layer, which depends on the hydrodynamic characteristics and conditions of the coolant inlet and outlet. Hydrodynamic characteristics of a single-phase fluid flow in porous structures, mainly in the region $\Pi_v \leq 0.5$, were studied in many experimental papers [41, 42]. In the general case, the hydrodynamics of the flow in porous structures is described by the modified Darcy's equation (Dupuit-Reynolds-Forchheimer equation) [43-45]:

$$-\frac{dp_0}{dx} = \alpha \mu_0 u + \beta \rho u^2, \quad (46)$$

where p_0 is the flow pressure; u is the filtration rate, equal to the ratio of the specific mass flow rate of the coolant G_0 to the density ρ ; α and β are the viscous

and inertial resistance coefficients, respectively; and μ_0 is coefficient of dynamic viscosity of the coolant.

From equation (46) we obtained the equation for the coefficient of friction, C_f , in the form

$$C_f = 2/(\text{Re} + 2), \quad (47)$$

where $C_f = -2(dp_0/dx)\rho/G_0^2\beta$ and $\text{Re} = G_0\beta/\mu_0\alpha$ (the characteristic size β/α).

Known also is a slightly different approach to the calculation of C_f : as a characteristic size use is made of \sqrt{K} , where K is the permeability coefficient, characterising the hydrodynamics of the flow according to Darcy's law ($\text{Re}_{\sqrt{K}} = G\sqrt{K}/\mu$), then

$$C_f = 2(1/\text{Re}_{\sqrt{K}} + c)/c. \quad (48)$$

The relationship between the coefficients α , β and parameters c and K can be represented as $\alpha = 1/K$ and $\beta = c/\sqrt{K}$. The parameter c is a universal constant for identical porous structures. For example, for all the materials made of metal powders with spherical or close-to-spherical particles $c \approx 0.55$, and for materials made of powders of arbitrary particle shape $0.45 < c < 0.566$. Thus, when calculating the hydraulic characteristics of the structures we assumed $c = 0.55$, although in our case this provides a somewhat higher value of the friction coefficient C_f .

The permeability coefficient K , which is a structural characteristic of a porous structure, does not depend on the flow regime and is determined experimentally from Darcy's law. In connection with the development of works in the field of heat pipes, many experimental data are currently available to determine K for powder and metal fibrous structures. The dependence of the permeability coefficient for metal fibrous structures on bulk porosity has the form [46]:

$$K = A\Pi_V^m, \quad (49)$$

where A and m are the coefficients depending on the relative length of the fibers l/d . Similar expressions can be obtained for powder porous structures. In addition, the permeability coefficient is calculated from the known Carman-Kozeny relation [41]:

$$K = \varphi\Pi_V^3 d_m^2 / (1 - \Pi_V)^2 \approx \Pi_V^3 / 5S_V, \quad (50)$$

where φ is a constant depending on the structure.

We used the expressions presented to determine the hydraulic characteristics of power optics elements utilising porous structures made of metal powders and metal fibrous structures.

d) *Effect of the coolant inlet and outlet conditions on the hydraulic characteristics of the POE*

Usually, in cooled POEs the coolant is supplied to and removed from the porous structure through evenly distributed alternating channels on the surface being cooled. In the case of inlets and outlets in the form of alternating holes we may deal with a significant nonuniformity of the velocity field in calculating the flow in radial directions. This leads to additional pressure drops in the circulation of the coolant, which are accounted for by the coefficient K_g . In this case, the total pressure drop in a porous structure has the form

$$\Delta P_0 = \Delta p_0 K_g, \quad (51)$$

where Δp_0 is the pressure drop in the case of a uniform velocity field.

The coefficient K_g , characterising the influence of collector effects on hydraulic resistance during the motion of the fluid in a porous structure, can be written as:

$$K_g = \frac{F}{\pi^2 n(1-a)} \frac{cG(1/a-1)/\pi\rho s\Delta - (v/\sqrt{K})\ln a}{v\sqrt{K} + cv}. \quad (52)$$

Here F is the area of the irradiated surface; n is the number of channels for the inlet (outlet) of the coolant; and $a = 2r_0/s$ is a relative spacing between the holes. One can see from equation (52) that K_g depends both on the geometric characteristics of the supply and removal of the coolant (on a) and on G ; with increasing a and G , the coefficient K_g increases. Thus, the coefficient K_g characterises the design excellence of the inlet and outlet system of the POE coolant.

When K_g is known, the total pressure drop in the porous structure is calculated by formula (51), taking into account the expression for calculating Δp_0 :

$$\Delta p_0 = v\rho s(1-a)(v/\sqrt{K} + cv)/\sqrt{K}, \quad (53)$$

where $v = Cs/(\rho F\Delta)$ is the coolant filtration rate.

e) *Thermal conductivity of porous structures in POEs*

As for the problems of cooling of POEs, of interest is to study the thermal conductivity of a porous structure skeleton. In most cases, data are summarised in the form of the dependence $\tilde{\lambda}(\Pi_V)$ for the samples, manufactured using the single technology and the same type of material. In calculations use can be made of the Odolevsky equation [47]:

$$\tilde{\lambda} = \lambda_c \frac{1 - \Pi_V}{1 + \Pi_V}, \quad (54)$$

where λ_c is the thermal conductivity of a compact material.

Effective thermal conductivity of metal fibrous felt structures may have a considerable anisotropy depending on the direction of the fibres in the felt. Usually, $\tilde{\lambda}$ is generalised by the relations [47]:

$$\tilde{\lambda}_{\parallel} = \lambda_c(1 - \Pi_V) \exp(-\Pi_V), \quad (55a)$$

$$\tilde{\lambda}_{\perp} = \lambda_c(1 - \Pi_V)^2, \quad (55b)$$

where $\tilde{\lambda}_{\parallel, \perp}$ is the effective thermal conductivity in the direction parallel and perpendicular to the felt-making plane. In the latter case one can also use the expression

$$\tilde{\lambda}_{\perp} = \lambda_c(1 - \Pi_V)^3. \quad (56)$$

$$W^* = \alpha_s \Delta_s t_T [1/2(\Theta_1 + \Theta_2) - \Theta_0] + \alpha_p \Delta_p t_T [(1 - \Theta_0) + \bar{q} d_m / (N' \Delta)], \quad (57)$$

where α_s and α_p are the temperature coefficients of linear expansion of the separating and porous layers, respectively; $\Theta_i = t_i / t_T$ is the dimensionless temperature; t_0 is the coolant temperature at the inlet of the reflector; and t_1 and t_2 are the temperatures of the outer and inner surfaces of the separating layer, respectively.

The above-derived expressions describing the processes of heat and mass transfer in porous structures were used to calculate the characteristics of cooled POEs.

Figure 3.7.12 shows the qualitative dependence of thermal deformation on the maximum density of the heat flow being removed (the variable Π_V at a constant d_m) for two selected regions of the reflector, corresponding to the regions of injection [$W_1^*(q_{lim1})$] and outflow [$W_2^*(q_{lim2})$] of the coolant. Varying the average grain size d_m (or the diameter of the fibre), we can construct a family of curves, characterised by a constant value of d_m and variable porosity V , for reflectors with the same type of the capillary structure. The curves were plotted at a constant pressure drop and by taking into account the coolant heating in the porous structure; in addition, the temperature of the coolant at the inlet was assumed equal to the POE temperature.

The expressions presented satisfactorily approximate the experimental data [40, 47] and can be used in the determination of the thermal characteristics of cooled POEs made of metal fibrous structures. In this case, expression (55b) describes the upper limit of the experimental data (an optimistic estimate), and (56) – the lower (a pessimistic estimate).

f) Thermal deformation of the optical surface

To assess small distortions of the optical surface, which are characteristic of POE deformation, we made an assumption of free expansion of the porous structure and the separating layer according to the temperature fields. Then, the thermal deformation of the mirror surface W^* is the sum of expansions of the separating (thickness Δ_s) and porous (thickness Δ) layers:

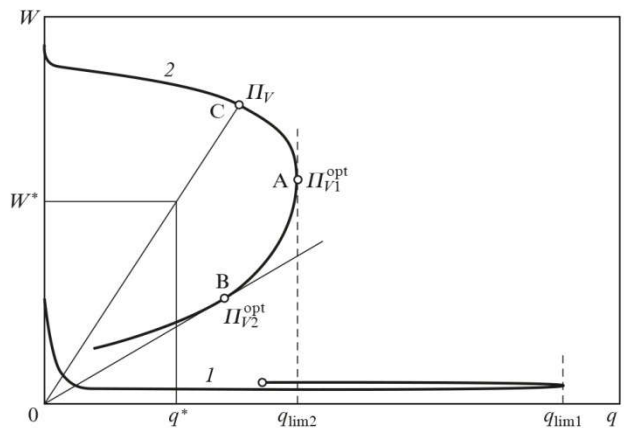


Figure 3.7.12: Qualitative dependence of thermal deformations on the maximum power density for the heat flow removed from two POE zones, corresponding to the regions of (1) injection and (2) outflow of the coolant

The deformation of the optical surface in the coolant outflow region is $W_2^* > W_1^*$; hence, crucial to the selection of the structural characteristics of the porous structure is curve (2), and the difference between curves (1) and (2) characterises the degree of perfection of the cooling system. The curves are the envelopes of the working thermal deformation characteristics of a family of reflectors with this type of structure. The performance characteristic of the reflector with a given porosity of the structure Π_V is obtained by connecting the straight line from point C with the origin of the coordinates. Point C corresponds to the maximum density of the heat flow, removed due to convective cooling, and the line segment OC is a dependence of

thermal deformations of the mirror surface on the heat load.

In general, curve (2) has two points: point A corresponding to optimal porosity Π_{V1}^{opt} which facilitates removal of the heat flow having the maximum density for the selected grain size, the coolant pressure drop, and coolant inlet and outlet conditions; and point B [the point of tangency of curve (2) with the straight line from the origin of the coordinates] corresponding to the porosity Π_{V2}^{opt} , for which in the porous structure the optimal thermal distortions of the mirror surface are realised.

The choice of material and the basic parameters of the structure (d_m and Π_V) must be based on a comparison of a family of curves (2) with possibilities of obtaining the desired porous structures and separating layers. In our review [14] we presented the results illustrating the feasibility of the experimental method and numerical calculations of thermal deformation characteristics of water-cooled POEs made of widely used copper and molybdenum powders.

g) *Liquid-metal coolants in POEs based on porous structures*

In 1978, we were first to suggest that a further increase in the optical damage threshold of mirror surfaces of POEs based on porous structures is possible when liquid alkali metals and their alloys are used as coolants [38]. Prospects of utilising liquid-metal coolants in POEs were determined by the possibility of achieving a high heat transfer coefficient in the porous structure due to a favourable combination of thermo-physical properties of liquid metals. This allowed one to lessen the requirements to the thermal conductivity of the porous structure material, which opened up the possibility of using new structural materials with a low thermal expansion coefficient and thermal conductivity in reflectors. Of particular interest was the employment

of eutectic alloys of liquid metals with low melting points in POEs.

Consider some results of theoretical and experimental investigations of heat and thermal deformation characteristics of POEs cooled by the eutectic alloy Na–K. As part of earlier assumptions the heat transfer equation can be written as

$$\frac{d^2t}{dx^2} = \frac{h_e}{\lambda} S_V (t - t_T), \quad (58)$$

where h_e is the heat transfer coefficient between the porous structure material and the coolant. Due to the lack of published data on the heat transfer of liquid metals in porous structures, the lower bounds of the heat transfer coefficient were estimated by using the known data on the heat transfer of liquid-metal coolants in triangular arrays of nuclear reactor fuel elements [48]. To calculate the heat transfer of liquid metals in the nuclear fuel assemblies, use was made of the relations: in densely packed structures ($s/d = 1$)

$$\text{Nu} = \text{Nu}_{\text{lam}} + 0.0408(1 - 1/\sqrt{1.24\varepsilon + 1.15})\text{Pe}^{0.65}; \quad (59)$$

in not densely packed structures ($1.0 < s/d < 1.2$)

$$\text{Nu} = \text{Nu}_{\text{lam}} + \frac{3.67}{90(s/d)^2} \times \left\{ 1 - \left[\frac{1}{[(s/d)^{30} - 1]/6 + \sqrt{1.24\varepsilon + 1.15}} \right] \text{Pe}^{m_1} \right\}; \quad (60)$$

in not densely packed structures ($1.2 < s/d < 2$)

$$\text{Nu} = \text{Nu}_{\text{lam}} + 3.67 \text{Pe}^{m_2} / 90(s/d)^2. \quad (61)$$

Here, $m_1 = 0.56 + 0.19s/d - 0.1/(s/d)^{80}$; Pe is the Peclet number;

$$\text{Nu}_{\text{lam}} = \left[7.55 \left(\frac{s}{d} - \frac{6.3}{(s/d)^{17(s/d)(s/d-0.81)}} \right) \right] \left[1 - \frac{3.6}{(s/d)^{20}(1 + 2.5\varepsilon^{0.86}) + 3.2} \right]$$

is the Nusselt number for the laminar flow; s/d is the relative spacing of the fuel elements in the array; and $\varepsilon = \lambda_{st} / \lambda_T$ is the ratio of the thermal conductivity of the fuel element cladding material to the thermal conductivity of the coolant. The relations (59)–(61) are valid for $\varepsilon > 0.01$ and $1 \leq \text{Pe} \leq 4000$.

Assuming that the hydraulic diameter of the array of the fuel elements corresponds to the hydraulic diameter of the POE porous structure ($d_s = d_p$), and the diameter of a set of rods – to the wire diameter (for metal-fibrous porous structures), we can obtain the dependence $d_s = d_m \Pi_V / (1 - \Pi_V)$ for felt porous structures.

Figures 3.7.13 and 3.7.14 show the results of numerical calculations of thermal deformation characteristics of the POE cooled by the eutectic coolant Na–K. It was assumed that the porous structures of the reflectors were made of molybdenum and invar felt. The mean diameter of the felt and the bulk porosity of the structure varied within $20 \leq d_m \leq 200 \mu\text{m}$ and $0.1 \leq \Pi_V \leq 0.9$. The curves in Figs. 3.7.13 and 3.7.14 are the envelopes of the thermal deformation characteristics of the POE family and plotted at a constant pressure drop of the coolant and a maximum temperature of the cooling surface equal to 100°C .

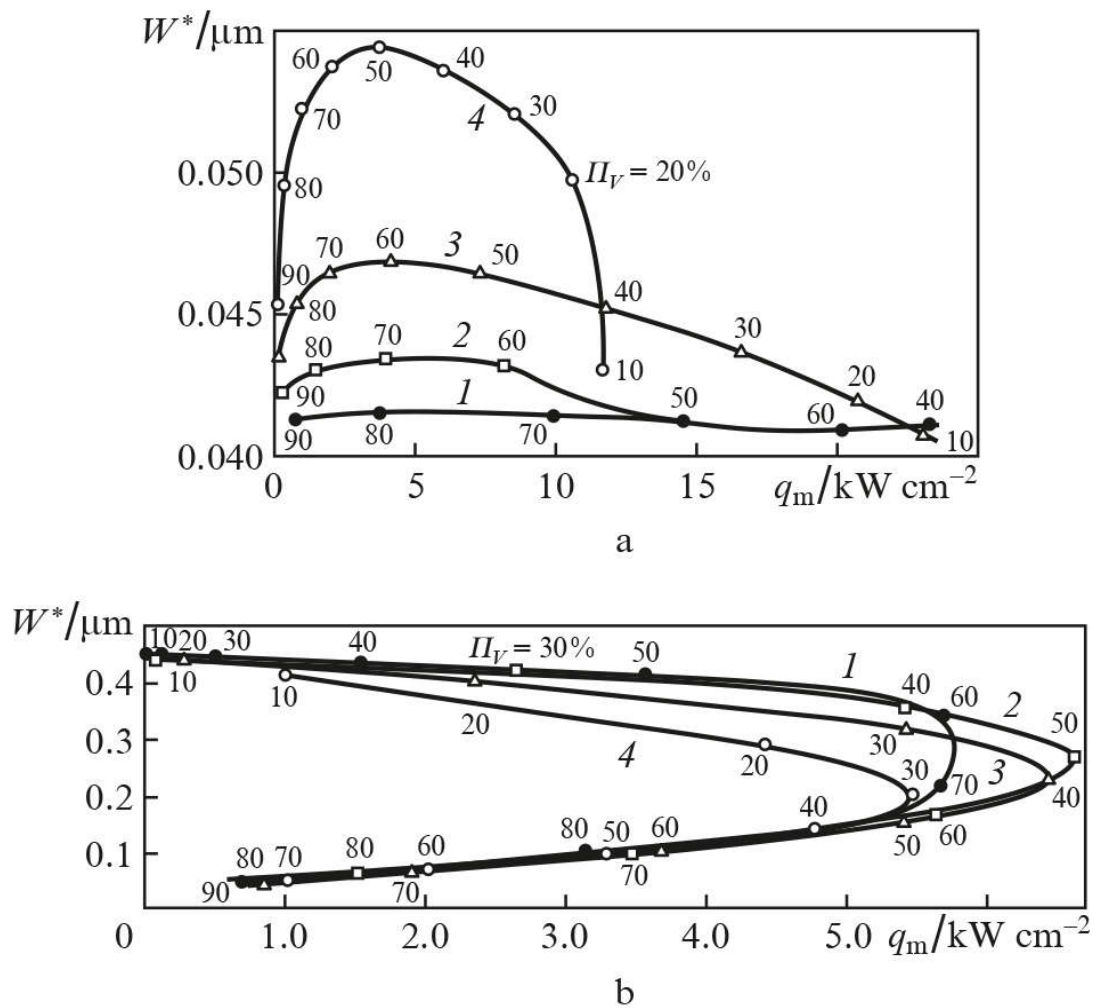


Figure 3.7.13: Nomograms of thermal deformation characteristics of POEs based on metal-fibrous porous structures made of molybdenum, which are cooled by a Na-K coolant in the regions of its inlet (a) and outlet (b) at $d_m =$ (1) 20, (2) 50, (3) 100 and (4) 200 μm .

One can see from Fig. 3.7.13 that the deformation of the optical surface in the region of the coolant outlet, calculated with account for its heating in the porous structure, substantially exceeds the deformation in the region of the coolant inlet ($W_2^* > W_1^*$). The maximum power densities of the heat flux for the POE in question are as follows: $q_1 > 20 \text{ kW cm}^{-2}$ in the region of the coolant inlet and $q_1 = 6.6 \text{ kW cm}^{-2}$ in the region of the coolant outlet; in this case, $W_2^* = 0.3 \mu\text{m}$. The minimum deformation W_2^* in the region of the coolant outflow at a power density of 4.2 kW cm^{-2} is 0.12 μm , which is significantly lower than the optical damage threshold of the POEs for CO_2 lasers.

Analysis of the data in Fig. 3.7.14 shows that the use of porous structures made of materials with a low thermal expansion coefficient (invar fibres) allows one to significantly (approximately by 3–4 times) reduce thermal deformations of the mirror surface both in the region of the coolant inlet and outlet in the case of liquid-metal cooling. Thus, the maximum thermal loads,

experimentally allocated from the mirror surface, exceeded 10 kW cm^{-2} . The experimentally measured thermal deformations of POEs made of invar fibres in the region of minimum deformations were less than 0.5 μm .

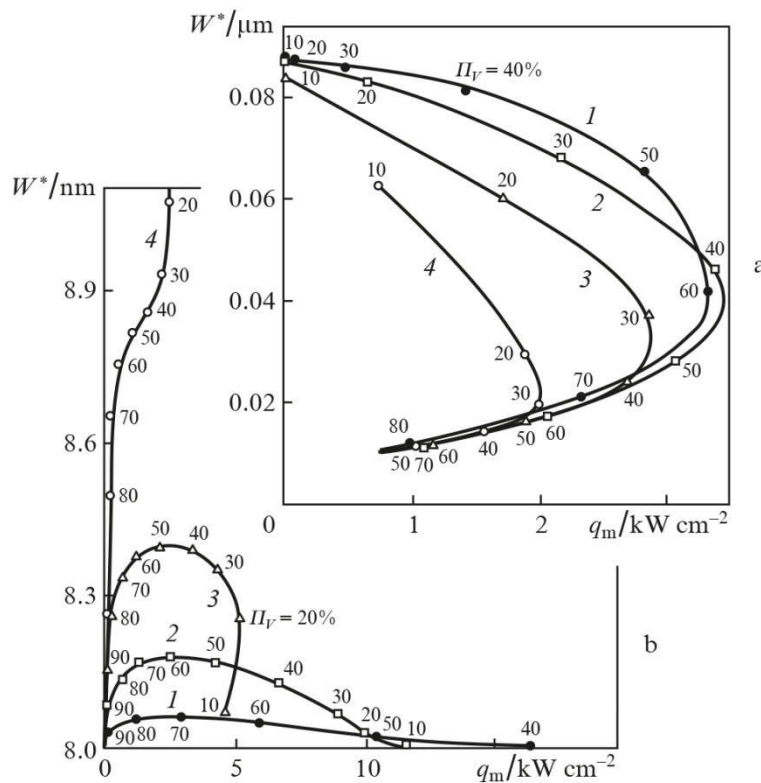


Figure 3.7.14: Nomograms of thermal deformation characteristics of POEs based on metal-fibrous porous structures made of invar, which are cooled by a Na–K coolant in the regions of its inlet (a) and outlet (b) at $d_m = (1) 20, (2) 50, (3) 100$ and (4) $200 \mu\text{m}$.

It should be noted that the results presented in Figs. 3.7.13 and 3.7.14 clearly show that liquid metals are very promising for POE cooling. Such cooling in combination with porous structures made of materials with relatively low coefficients of thermal expansion opens up fundamentally new possibilities for creating a class of very precise POEs with a high optical damage threshold.

Today, due to the accumulation of experimental data on convective heat transfer and hydrodynamics in porous structures, such structures are widely used in space instrumentation and nuclear power systems exposed to high radiation doses. Due to the structural features, metal porous structures have no blind pores, which eliminates unwanted thermal processes. They provide good permeability, high thermophysical characteristics, ability to use POEs at a boiling point of working fluids in heated regions, high heat transfer rates and high limiting values of critical heat fluxes. Metal porous structures exhibit good physicochemical and performance characteristics. Metallurgical production technology ensures their stability and reproducibility, long service life, and high reliability. One of the first mirrors based on porous structures is shown in Fig. 3.7.15.

The new areas of research, which have been successfully developed recently, include the study of boiling on surfaces with porous coatings with their

structural and hydrodynamic characteristics taken into account, the study of the influence of these characteristics on the contact thermal resistance between the porous and solid layers, and the study of heat transfer during condensation of liquids on the working surfaces of porous structures. It should be noted that our investigations of heat transfer in porous structures made it possible to develop the technological basis for creating a series of water-cooled mirrors for power lasers by employing chemical etching of metal foils with subsequent soldering to fabricate a multilayer heat exchanger with a moderate degree of development of the heat exchange surface [49–52].

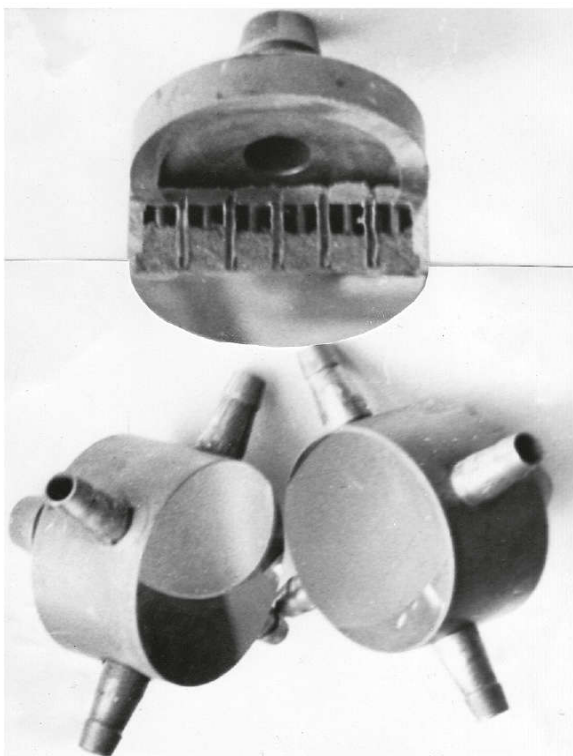


Figure 3.7.15: Cooled POE with a powder porous structure

IV. ADAPTIVE POES AND OPTICAL SYSTEMS BASED ON THEM

The variety of the phenomena that change the optical characteristics of the medium in the propagation path of radiation and in the optical system of the laser leads to degradation of the quality of the wavefront (WF), which is manifested by a significant increase in the angular divergence of the generated beam and by a reduction in the peak intensity upon focusing. Most fully the entire range of requirements to WF correctors in adaptive optics systems is met by POEs with adjustable shape of the reflecting surface, in which the WF distortion are compensated for by changing the shape of the mirror surface. In this case it is possible: 1) to fabricate cooled and uncooled adaptive POEs with a high optical damage threshold in a wide range of radiation exposures [21, 53]; 2) to produce adaptive optics systems for the entire set of currently known schemes for generation of cw and repetitively pulsed laser radiation in wavelengths ranging from far-IR to ultraviolet; and 3) to manufacture adaptive POEs for correcting and measuring non-stationary phase distortions in the time interval up to several milliseconds, by selecting the substrate materials of the mirror surface which provide their predetermined static and dynamic deformation properties [54–56].

The most challenging, in our view, is the realisation of adaptive POEs with a high optical damage threshold of the reflecting surface, because it is necessary in this case to combine the shape and

cooling control systems in the reflector. Our approach to creating adaptive POEs was based on the methods of forced heat removal for cooling the mirror surface while shaping the reflecting surface by controlled elastic deformation of the porous structure of the heat exchanger.

Prospects of our proposal consisted in the possibility of providing the necessary static and dynamic deformation and thermal characteristics of adaptive POEs, because the use of porous structures allows one to implement the optical damage threshold (up to several tens of kW cm^{-2}) of the mirror surface, whereas their use as a substrate material of the mirror surface having low stiffness enables control of the shape of the reflecting surface in a wide range of local displacement amplitudes of its individual regions. Moreover, since in the operating condition the material of the porous heat exchanger of an adaptive POE is filled with a liquid coolant, natural resonant oscillations of the mechanical design of the adaptive POE may be effectively damped in the dynamic regime of the device operation.

Studies on modelling the correction of basic WF distortions by the adaptive POE, determining the optical quality of the intense laser radiation flux (including the WF tilt, defocusing, spherical aberrations), showed that at a consistent satisfaction of the power optics requirements, involving realisation of high values of the optical damage threshold (the porous structure thickness of the exchanger must be several millimetres), inaccuracy of conjugation of the WF shape with the shape of the reflecting surface for CO_2 laser radiation is $\lambda_0/10 - \lambda_0/20$ using a control system with 50–60 actuators on the aperture of the adaptive POE up to 100 mm in length.

Along with the well-known solutions [56, 57], our approach to creating adaptive POEs is very promising in the development of adaptive optics systems for high-power lasers [58–63]. However, its implementation required complex investigations to establish the peculiarities of dynamic and static regimes of deformation of porous structures, to study the influence of the processes of internal friction in porous materials on the dynamics of their cyclic loading, to determine the effect of anisotropy of mechanical properties of the structure on the form of the response function of the reflecting surface, to establish an optimal (for these devices) control of an adaptive optical system, and to create new types of actuators with high energy capacity. It is important to note the major role of the design bureaus headed at that time by B.V. Bunkin and N.D. Ustinov in achieving these goals.

Great importance in the development and creation of adaptive POEs with specified static and dynamic characteristics was given to actuators providing the required amplitudes of deformation over a wide dynamic range. Solutions related to the use of

piezoelectric materials in physical problems associated with adaptive POEs are not free from drawbacks. These include the need for high strains required for the realisation of amplitude displacements and the inevitability of hysteresis phenomena that hinder the formation of a phase-conjugated laser beam WV by the relief of the reflecting surface. In the regimes of 'modulation' and 'phase conjugation' the amplitudes of local displacements of the reflecting surface should reach $0.1-0.5\lambda_0$ and $1-5\lambda_0$, respectively. To ensure such displacement amplitudes we proposed adaptive POE actuators of new types, which are made of magnetostrictive materials and implement the conditions for the Joule and Wiedemann effects [62, 63]. At the same time we pointed out the prospect of creation of compact highly efficient actuators, providing a stable amplitude displacement in the frequency range up to 10 kHz.

The employment of the designed and built adaptive POEs utilising porous structures is not confined to adaptive optics, although in this field they solve a number of important problems. According to the results of modelling intracavity optical systems [64-68], the use of adaptive POEs allows one to obtain the diffraction angular divergence of radiation fluxes when use is made of unstable resonators in high-power carbon dioxide laser systems. Adaptive POEs were essentially a new type of devices ensuring the local control of phase characteristics of coherent radiation fluxes. As a result, they served as prototypes for different laser beam modulation, selection and scanning devices. For example, the use of an adaptive POE in the laser cavity made it possible to convert high-power cw radiation into high-frequency repetitively pulsed radiation by Q-switching [68], and the employment of adaptive POEs in a Fabry-Perot interferometer allowed for automated analysis of spectral and modal composition of laser radiation, etc. Undoubtedly are the advantages of this class of adaptive POEs in traditional applications of adaptive systems, such as laser ranging. Here we should mention paper [57], which presents the characteristics of a number of adaptive mirrors.

V. LARGE POES BASED ON MULTILAYER HONEYCOMB STRUCTURES

Actual operating conditions of large POEs put forward in most cases contradictory requirements, significantly complicating the process of their manufacture. With low weight and high specific stiffness, large POEs should continue to operate under intense unilateral heating and rapidly changing ambient temperature. However, increasing the size of the POEs, while preserving the predetermined level of the optical surface distortion, dramatically increases their mass. To reduce the weight of large POEs while maintaining the

stiffness of their structures, along with new approaches such as the use of materials with synthesised physical and technical properties promising is also the search for new solutions to the problem. In some cases, the POE weight is reduced by creation of internal voids with relatively large cells. This allows one to decrease the POE weight by 6-7 times for the value of optical surface distortion by its own weight, which is 0.7-0.8 of monolithic mirror distortion. However, it is difficult to create a system of thermal stabilisation without significant loss of rigidity in POEs with large internal voids.

An alternative way to reduce the weight of bulky POEs, as in the case of highly loaded POEs, is the use of highly porous honeycomb materials [69, 70]. We theoretically and experimentally investigated the possibility of creating lightweight bulky POEs based on multilayer honeycomb structures. Such structures have a relatively small mass at high specific stiffness, good thermal insulation properties and high absorption of elastic vibrations. Multilayer structures also provide the ability to create a highly efficient system of thermal stabilisation.

In the case of axisymmetric thermal loading the problem of thermal distortions of the optical surface of a cooled multilayer honeycomb POE was solved in [71]. In this case, to calculate the temperature fields in a large POE, we considered the problem for a multilayer cylinder whose end and side surfaces were heated, and inside the layers the heat was removed by a coolant. Thermal deformations W^* of the optical surface were determined as the sum of the normal thermal expansion of the POE and its bending

$$W^* = W_n^* + W_{\text{bend}}^*, \quad (62)$$

where $W_n^* = \int_0^H \beta(z)T(z, r)dz$ is the normal extension;

$\beta(z)$ is the linear expansion coefficient; $T(z, r)$ is the temperature; and H is the POE thickness.

Bending was determined from the equation

$$\nabla^4 W_{\text{bend}} = -\nabla^2 \frac{M_T}{D},$$

where

$$M_T = \int_{z_0-H}^{z_0} \frac{E\beta z}{1-\nu} T(z, r)dz$$

is the temperature moment;

$$D = \int_{z_0-H}^{z_0} \frac{Ez^2}{1-\nu} dz$$

is the bending stiffness; and E is Young's modulus. Poisson's ratio $\tilde{\nu}$ and the position of the neutral surface were determined from the conditions

$$\int_{z_0-H}^{z_0} \frac{E}{1-\nu^2} (\tilde{\nu} - \nu) dz = 0, \quad \int_{z_0-H}^{z_0} E z dz = 0,$$

$$W_{\text{bend}}(r) = C_1 + C_2 \ln r + C_3 r^2 + C_4 r^2 \ln r + \frac{1}{D} \int_0^2 \frac{1}{\rho} \int_0^\rho \xi H(\xi) d\xi d\rho, \quad (63)$$

and the constants C_1, C_2, C_3 and C_4 - from the boundary conditions.

Studies showed [72, 73] that for the absorbed heat flux equal to $\sim 10 \text{ W cm}^{-2}$ the optical surface distortions of the POE based on multilayer honeycomb invar structures do not exceed $0.7 \mu\text{m}$ at the POE diameter of 1 m. Constant thermal stabilisation (time needed to reach steady-state operation), which is determined from the solution of the nonstationary problem, for such structures is a few tenths of a second. A peculiar feature of lightweight honeycomb POEs is the fact that a relatively non-rigid filling material may experience a shear strain and transverse compression, significantly affecting the POE operation. In this connection, there appeared a problem of its optimisation, which was considered in the framework of nonlinear programming. The relative displacement of the POE surface under the influence of gravitational, mechanical and thermal loadings was determined by the finite element method [73].

Figure 3.7.16 shows the dependence of M^*/M and H^*/H on the allowable distortion W^* of the optical surface of the POE under its own weight. Here M^* and H^* are the weight and thickness of a circular monolithic plate, and M and H are the weight and thickness of the three-layer honeycomb invar structure with a diameter of 2 m. It can be seen that the effectiveness of the multilayer honeycomb structure increases with toughening the requirements for an acceptable distortion of the optical surface. Figure 16 also shows that for certain ratios of the structural parameters, the optical surface distortion can be minimised. The example of employment of multilayer honeycomb structures during the manufacture of large POEs 1 m in diameter is shown in Fig. 3.7.17. Lightweight bulky POEs made of invar are currently used in laser facilities and confirm their high efficiency. This class of POEs is described in detail in [74].

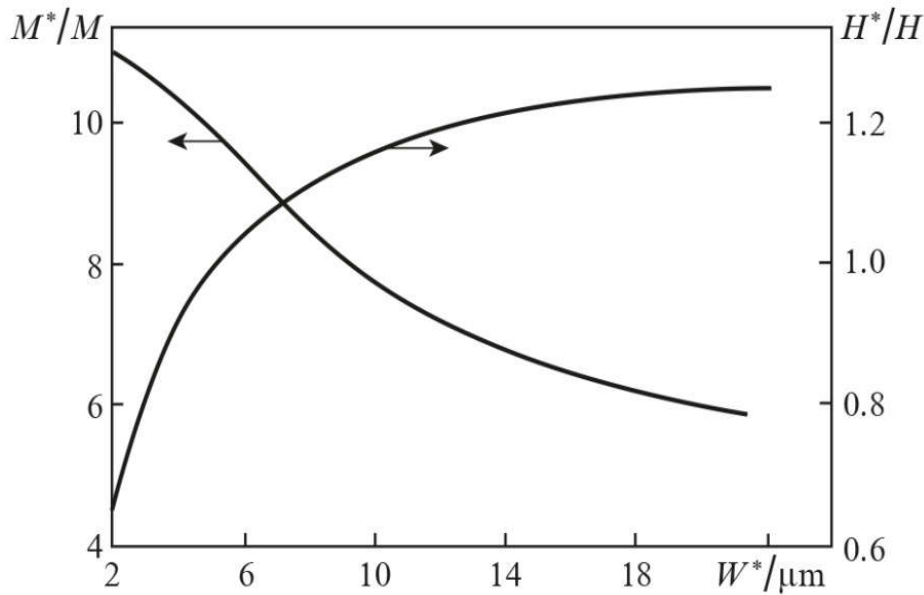


Figure 3.7.16: Dependences of the thickness and weight of a bulky honeycomb invar POE 2 m in diameter on distortions of the optical surface

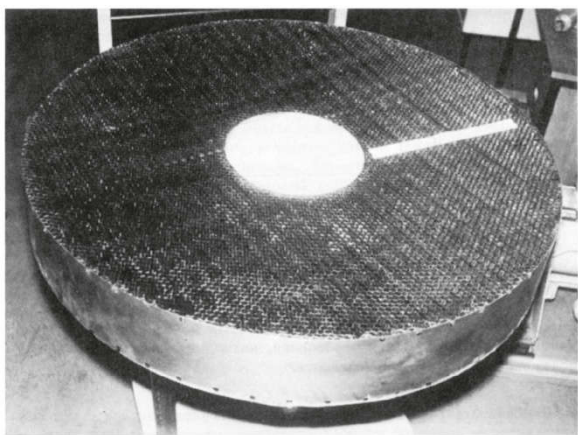


Figure 3.7.17: Preform of a large multilayer honeycomb invar POE 1 m in diameter

VI. LARGE POES BASED ON COMPOSITE MATERIALS

Progress in this area is largely provided by the rapid development of new technologies and the synthesis of materials with fundamentally new properties. The need for such a development is associated with an ever-expanding range of problems faced by modern science and practice.

A common disadvantage of large POEs made of glass, glass ceramics, fused quartz and other materials, which are used in optical astronomy and laser technology, is their low thermal conductivity. Such mirrors cannot be used effectively in unilateral heating and technological features of their production do not allow one to significantly reduce weight and ensure effective thermal stabilisation.

Good results in the fabrication of lightweight large POEs have been achieved using composite materials, the methods of their manufacture being well developed [75–78]. Of greatest interest is the silicon infiltrated carbon-fibre-reinforced silicon carbide composite. The process is based on the deposition of carbon on a free surface during gas phase pyrolysis. Precipitating carbon strengthens frame filaments and combines them into a rigid three-dimensional lattice. The thus obtained porous silica preforms are impregnated with silicon melt in an inert atmosphere. By varying the amount of silicon and impregnation temperature, one can produce samples, significantly different in porosity and phase composition. One can also fabricate virtually carbide porous structures with advanced open porosity, which, except for weight reduction, provides an effective system for thermal stabilisation. Heat treatment removes residual stresses in the composite, increasing its structural stability.

A significant weight reduction of POEs while maintaining their specific rigidity can be achieved also by creating a honeycomb structures. For a honeycomb frame to be manufactured, we used the slip-casting

method. Specially prepared slip mass was poured into a mold and polymerised. After removal of the mold the preform was annealed and siliconized.

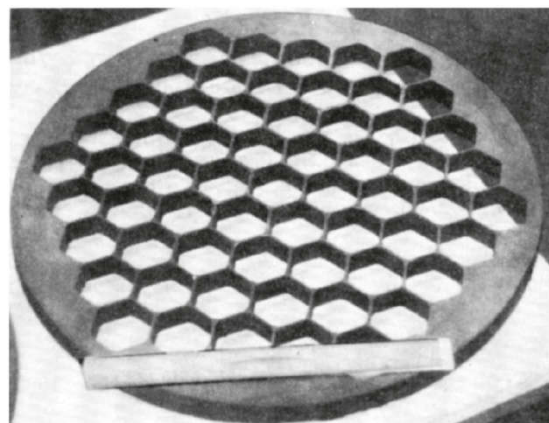


Figure 3.7.18: Honeycomb frame of the POE

Figure 3.7.18 shows a honeycomb frame, produced by the slip-casting method. By joining the resultant honeycomb frame with monolithic plates made of the same material one can form a multilayer honeycomb structure with highly efficient thermal stabilisation.

Figure 3.7.19 shows a photograph of a lightweight uncooled POE 500 mm in diameter, placed on a polishing/lapping machine. A highly reflecting coating was deposited on the optical surface of the silicon carbide wafer having a surface roughness of $0.010 \mu\text{m}$.

The optical damage threshold of cooled and uncooled POEs based on silicon infiltrated carbon-fibre-reinforced silicon carbide composites was measured experimentally, high power densities being simulated by the electron beam heating facility we developed [79–81]. The POE was installed in a vacuum chamber and served as an anode of an electro-optical system. The optical damage threshold of the cooled POE 500 mm in diameter was achieved under thermal loading by an electron beam with a power density of $\sim 300 \text{ W cm}^{-2}$, which at characteristic values of the reflection coefficients of the POE materials for laser radiation is equivalent to a power density up to a few tens of kW cm^{-2} . Significant expansion of the range of new materials and the development of modern processing methods and technologies of their connection favours the manufacture of effective large POEs made of C/SiC materials based with record-high thermal stabilisation and high optical performance.

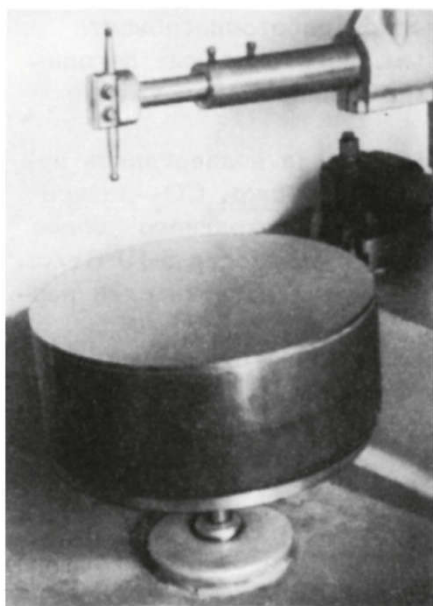


Figure 3.7.19: Large POE 500 mm in diameter on a polishing machine

VII. HIGH POWER/ENERGY OPTICS AND ITS NEW APPLICATIONS

a) Cooling of laser diode assemblies

One of the brightest and most promising implementations of the ideas of power optics is now the introduction of forced heat transfer in high power/energy semiconductor lasers, which are widely used today to pump solid-state lasers having active elements of different geometry: rods, disks, slabs, fibres [82–86]. Solid-state lasers have the highest efficiency reaching 80% in some case. Modern manufacturing technologies of semiconductor structures made it possible to significantly increase the laser lifetime (tens of thousands of hours of continuous operation). The variation of the semiconductor material composition can change the wavelength range of radiation from the near-IR to the UV. These lasers are very compact, reliable and easy to operate. The power output can be increased by the simultaneous use of a large number of laser diodes, which are formed in one-dimensional or two-dimensional effectively cooled structures (Fig. 3.7.20).

Cooled laser diode assemblies possess almost all the remarkable properties of single semiconductor lasers: high intensity, high reliability and long lifetime. These lasers have much smaller weight and size dimensions in comparison with other types of lasers, can easily be fed from independent low-voltage power supplies (solar, nuclear energy) without bulky transformers. Equipment based on laser diode assemblies really becomes a reliable high-performance instrument that can be used in industry, medicine, research and military applications.

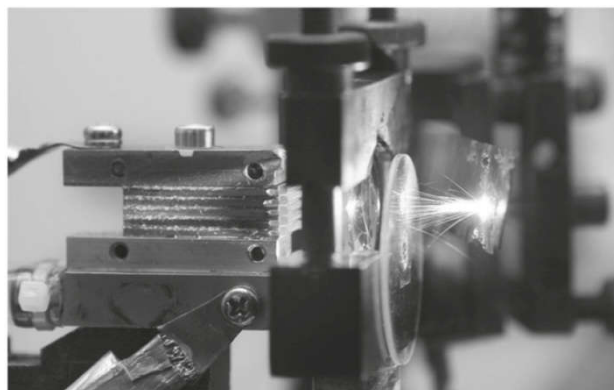


Figure 3.7.20: Cooled laser diode assembly

The stability of operation of laser diode assemblies and the value of their output are completely determined by the heat transfer efficiency. Laser diode arrays are soldered with a low-temperature solder to the surface of the heat exchanger, which is produced in accordance with high-power optics technology. It should be noted that the levels of heat fluxes which are to be removed from the contact region of the array with the heat exchanger have already approached the characteristic values of the power optics and are equal to several hundreds of W cm^{-2} .

b) New generation of high power/energy optics based on silicon carbide

Currently, the development of high-power optics stimulates three trends of efficient use of its technical and technological solutions:

- Lightweight, highly stable, large ground- and space-based telescopes for studying the universe and transmitting energy over long distances;
- Astronomical optical instruments for remote sensing of the Earth and near space from spacecrafts;
- Highly efficient cooled POEs for high-power lasers and laser systems.

All the three trends are based on cutting-edge technologies. The choice of the POE material is a key issue in production of a new generation of optical objects. Thus, a bulky silicon carbide POE has a weight that is 7–10 times lower than that of the POE made of glass ceramics, the best quality in terms of radiation scattering, high thermal stability and a minimum time constant (Fig. 3.7.21). Comparative evaluation of materials with the help of optical quality criteria developed by us in the early 1970s showed that silicon carbide has a distinct advantage over traditional materials [19, 20]. This conclusion is consistent with more recent conclusions of foreign experts from Germany, France, Japan and China. It is appropriate here to note the contribution of acad. E.P. Velikhov, who initially supported the creation of the technology of silicon carbide production and the development of large optics.

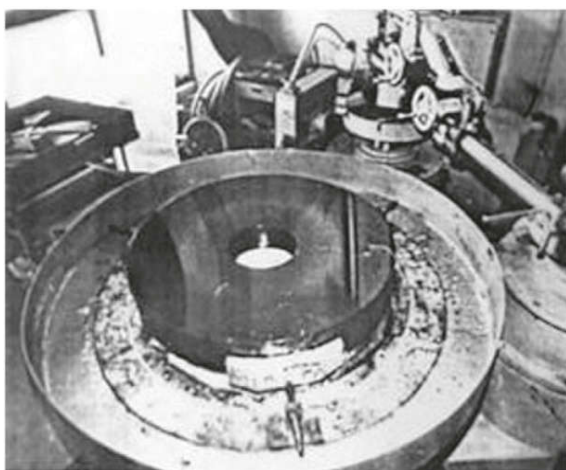


Figure 3.7.21: Silicon carbide POE

Obviously, the development of bulky POEs for high power/energy lasers and transition to a new generation of space-based telescopes is accompanied by the introduction of silicon carbide and related technologies into everyday practice.

VIII. CONCLUSIONS

In concluding this chapter of theoretical and experimental works in the field of high power/energy optics we should note one very important point: Effective development of any of the areas of modern cutting-edge technologies, as a rule, gives a result not only in the related fields of technological applications, but also in completely different branches of science and technology. Thus, the appearance of one- and two-dimensional cooled high-power laser diode arrays, large astronomical cooled POEs based on silicon carbide and complex composite materials is largely a consequence of the success of power optics [94–99] – a recognized effective donor for many areas of science and advanced technology of the XXI century. Its successful development continues.

REFERENCES RÉFÉRENCES REFERENCIAS

1. Barchukov A.I., Karlov N.V., Konyukhov V.K. Konev Yu.B., Krynetskii B.B., Marchenko V.M., Petrov Yu.N., Prokhorov A.M., Skobel'tsyn D.V., Shirkov A.V. *Otchel FIAN* (FIAN Report) (Moscow, 1968-1970).
2. Barchukov A.I., Konev Yu.B., Prokhorov A.M. *Radiotekh. Electron.*, 15, 2193(1970).
3. Barchukov A.I., Konev Yu.B., Prokhorov A.M. *Radiotekh. Electron.*, 16, 996 (1971).
4. Apollonov V.V., Barchukov A.I., Konyukhov V.K., Prokhorov A.M. *Otchel FIAN* (FIAN Report) (Moscow, 1971).
5. Apollonov V.V., Barchukov A.I., Konyukhov V.K., Prokhorov A.M. *Otchel FIAN* (FIAN Report) (Moscow, 1972).

6. Apollonov V.V., Barchukov A.I., Konyukhov V.K., Prokhorov A.M. *Pis'ma Zh. Eksp. Teor. Fiz.*, 15, 248 (1972).
7. Apollonov V.V., Barchukov A.I., Prokhorov A.M., *Proc. First Europ. Conf. 'Lasers and applications'* (Drezden, GDR, 1972).
8. Apollonov V.V., Barchukov A.I., Konyukhov V.K., Prokhorov A.M. *Kvantovaya Elektron.*, No. 3 (15), 103 (1973) [*Sov. J. Quantum Electron.*, 3 (3), 244 (1973)].
9. Apollonov V.V., Barchukov A.I., Prokhorov A.M. *Proc. Second Europ. Conf. 'Lasers and applications'* (Drezden, GDR, 1973); Preprint FIAN No. 157 (Moscow, 1973).
10. Apollonov V.V., Barchukov A.I., Prokhorov A.M., *Otchet FIAN* (FIAN Report) (Moscow, 1973).
11. Glass A J., Guenther A.H. *Appl.Opt.*, 12, 34 (1973).
12. Cytron S.J. *Memorandum Report M73-I7-1* (Philadelphia, PA, 1973).
13. Jacobson D.H., Bickford W., Kidd J., Barthelemy R., Bloomer R.H. *AIAA paper No. 75-779*(1975).
14. Apollonov V.V. *Laser Phys.*, 23, 1 (2013).
15. Apollonov V.V., Barchukov A.I., Prokhorov A.M. *Radiotekh. Electron.*, 19, 204 (1974).
16. Apollonov V.V., Barchukov A.I., Prokhorov A.M. *IEEE J. Quantum Electron.*, 10, 505 (1974).
17. Apollonov V.V., Preprint FIAN No. 105 (Moscow, 1973).
18. Barchukov A.I. *Doct. Diss.* (Moscow, FIAN, 1974).
19. Apollonov V.V., Barchukov A.I., Prokhorov A.M., *Kvantovaya Elektron.*, 2, 380 (1975)
20. Apollonov V.V. *Cand. Diss.* Moscow, FIAN, (1975).
21. Apollonov V.V. *Doct. Diss.* Moscow, FIAN, (1982).
22. Parkus H. *Instalionare Warmespannyngen* Wien: Springer, 1959; Moscow: Fizmatgiz, (1963).
23. Nowacki W. *Problems of Thermoelasticity* (Warszawa: PWM-Polish Scientific Publishers, 1960; Moscow: Izd. AN SSSR, (1962).
24. Jahnke E., Ernde F., Losch F. *Tafeln Hoherer Funktionen* (Stuttgart: Verlagsgesellschaft, 1960; Moscow: Nauka, (1964).
25. Tsesnek L.S., Sorokin O.V., Zolotukhin A.A. *Metallicheskie zerkala*, Moscow: Mashinostroenie, (1983).
26. Apollonov V.V., Bunkin F.V., Chetkin S.A. *Tez. Dokl. I Vsesoyuz. Konf. 'Problemy upravleniyaparametrami lazernogo izlucheniya'* Proc. I All-Union Conf. on Problems of Controlling Parameters of Laser Radiation) (Tashkent, (1978).
27. Apollonov V.V., Barchukov A.I., Prokhorov A.M. *Tez. Dokl V Vsesoyzn. Soveshchaniya po neresonansnomu vzairnodeistviyu opticheskogo izlucheniya s veshchestvom* (Proc. V All-Union Meeting On Nonresonant Interaction of Optical Radiation with Matter) (Leningrad, (1978).
28. Bennet H.E., Porteus J.O. *J. Opt. Soc. Am.*, 51, 123 (1961).

29. Apollonov V.V., Prokhorov A.M., Chetkin S.A. *Kvantovaya Elektron.*, 8, 2208 (1981).
30. Apollonov V.V., Bystrov P.I., Goncharov V.F., Prokhorov A.M. *Aulh. Cert. No. 135237*(priority date 08.12.1978).
31. Yokobori T. *An Interdisciplinary Approach to Fracture and Strength of Solids* (Groningen: Wolters-Noordhoff, 1968; Moscow: Mir, 1971).
32. Apollonov V.V., Barchukov A.I., Prokhorov A.M., *Otchet FIAN* (FIAN Report) (Moscow, 1977).
33. Apollonov V.V., Barchukov A.I., Prokhorov A.M., *Auth. Cert. No. 103162* (priority date 24.05.1977).
34. Apollonov V.V., Barchukov A.I., Prokhorov A.M., et al. *Kvantovaya Elektron.*, 5, 1169 (1978) [*Sov. J. Quantum Electron.*, 8, 672 (1978)].
35. Apollonov V.V., Barchukov A.I., Prokhorov A.M., et al. *Auth. Cert. No. 135238* (priority date 08.12.1978).
36. Apollonov V.V., Barchukov A.I., Prokhorov A.M. *Auth. Cert. No. 144371* (priority date 19.01.1979); Apollonov V.V., Prokhorov A.M., et al. *Auth. Cert. No. 142696* (priority date 29.06.1979).
37. Apollonov V.V., Barchukov A.I., Prokhorov A.M. *Proc. Laser Opt. Conf.* (Leningrad, 1980) p. 43.
38. Apollonov V.V., Prokhorov A.M. *Kvantovaya Elektron.*, 8, 1328 (1981) [*Sov. J. Quantum Electron.*, 11, 796 (1981)].
39. Apollonov V.V., Prokhorov A.M. *Kvantovaya Elektron.*, 8, 1331 (1981)[*Sov. J. Quantum Electron.*, 11, 798 (1981)].
40. Isachenko V.P., Osipov V.A., Sukomel A.S. *Teploperedacha* (Heat Transfer) (Moscow: Energiya, 1969).
41. Mayorov V.A. *Teploenergetika*, (1), 64 (1978).
42. Kays W.M., London A.L. *Compact Heat Exchangers* (New York: McGraw Hill, 1984; Moscow: Energiya, 1967).
43. Dupuit J. *Eludes Theoretiques et Pratiques sur le Movement des Eaux* (Paris, 1863).
44. Deitrich P. et al. *Flow and Transport in Fractured Porous Media* (Berlin: Springer-Verlag, 2005).
45. Forcheimer P. *Vereines deutscher Ingenieure*, 45 (1901).
46. Beavers G.S., Sparrow E.M. *Journal of Applied Mechanics*, 36, 711 (1969).
47. Belov S.V. *Poristye materialy v mashinostroenii* (Porous Materials in Mechanical Engineering) (Moscow: Mashinostroenie, 1967).
48. Subbotin V.I., Ibragimov M.Kh., Ushakov P.A. *Gidrodinamika i teploobmen v atomnykh reactorakh* (Hydrodynamics and Heat Exchange in Nuclear Reactors) (Moscow: Atomizdat, 1975).
49. Apollonov V.V., Bunkin B.V., Zakhar'ev L.N., Polyashev N.N., Prokhorov A.M. *Auth. Cert.No. 152944* priority date 14.02., (1980).
50. Khomich V.Yu. *Cand. Diss.* (Moscow, FIAN, 1981).
51. Apollonov V.V. et al, *Kvantovaya Elektron.*, 8, 2208 (1981)
52. Voinov Yu.P. *Cand. Diss.* Moscow, NPO 'Almaz', (1982).
53. Chetkin S.A. *Cand. Diss.* Moscow, FIAN, (1983).
54. Apollonov V.V., Prokhorov A.M. *Izv. AkadNauk SSSR. Ser. Fiz.*, 8, 48, (1984).
55. Apollonov V.V., Chetkin S.A., Prokhorov A.M. *Proc. Boulder Laser Damage Symp. XVI* (USA, NBS-Boulder, Colorado, 1984).
56. Safronov A.G. *Cand. Diss.* Moscow, GPI, (1996).
57. Shanin O.I. *Shirokoaperturnaya silovaya adaptivnaya optika* (Wide-Aperture Adaptive Power Optics) (Moscow: Fotonika, 2012).
58. Apollonov V.V., Chetkin S.A. *Kvantovaya Elektron.*, 15, 2578 (1988) [*Sov. J. Quantum Electron.*, 18, 1621].
59. Apollonov V.V., Prokhorov, *Pis'ma Zh. Tekh. Fiz.*, 14, 3 (1988).
60. Apollonov V.V., Prokhorov A.M. et al, *Kvantovaya Elektron.*, 18, 358 (1991) [*Sov. J. Quantum Electron.*, 21, 325 (1991)].
61. Apollonov V.V., Prokhorov A.M. *Proc. Boulder Laser Danuige Symp. XX* (USA, NBS-Boulder, Colorado, 1989).
62. Apollonov V.V., Borodin V.I., Brynskikh A.S., Zienko S.I., Murav'ev S.V., Temnov S.N. *Kvantovaya Elektron.*, 16, 386 (1989)
63. Apollonov V.V., Prokhorov A.M. *Kvantovaya Elektron.*, 17, 1496 (1990)
64. Apollonov V.V., Artemov D.V., Kislov V.I. *Kvantovaya Elektron.*, 1203 (1993)
65. Apollonov V.V., Artemov D.V., Kislov V.I. *Kvantovaya Elektron.*, 577 (1994)
66. Apollonov V.V., Kislov V.I. *Kvantovaya Elektron.*, 23, 999 (1996)
67. Apollonov V.V., Kislov V.I., Prokhorov A.M. *Kvantovaya Elektron.*, 23, 1081 (1996)
68. Apollonov V.V., Kislov V.I., Suzdaltsev A.G. *Kvantovaya Elektron.*, 33, 753 (2003)
69. Apollonov V.V., Prokhorov A.M., *Pis'ma Zh. Tekh. Fiz.*, 14, 236 (1988).
70. Apollonov V.V. et al, *Pis'ma Zh. Tekh. Fiz.*, 15, 3 (1989).
71. Apollonov V.V., Prokhorov A.M., Babayants G.I., *Pis'ma Zh. Tekh. Fiz.*, 16, 2 (1990).
72. Apollonov V.V., Prokhorov A.M., *Pis'ma Zh. Tekh. Fiz.*, 17, 655(1991).
73. Shmakov V.A. *Doct. Diss.* Moscow, GPI, (1997).
74. Shmakov V.A. *Silovaya optika* Moscow: Nauka, (2004).
75. Alekseev V.A., Antsifirov V.N., Apollonov V.V., Bilibin S.V., Gadzhiev M.G., Kunevich A.P., Narusbek E.A., Prokhorov A.M. *Pis'ma Zh. Tekh. Fiz.*, 11, 1350, (1985).
76. Apollonov V.V., Kolesov V.S., Prokhorov A.M., et al. *Pis'ma Zh. Tekh. Fiz.*, 16, 79, (1990).
77. Apollonov V.V., Babayants G.I., Gartman M.V., Golomazov V.M., Loktionov Yu.D., Pirogova Yu.M.,

- Plotsev G.V., Prokhorov A.M. *Pis'ma Zh. Tekh. Fiz.*, 16, 83, (1990).
78. Apollonov V.V. *Tech. Dig. 'Lasers 2001' USA*, Tucson, Arizona, (2001).
79. Apollonov V.V., Prokhorov A.M., Auth. Cert. No. 4250382 priority date 17.03. (1987).
80. Shurygin V.A. *Cand. Diss.* Moscow, NPO Almaz', (1992).
81. Apollonov V.V. et al, *Proc. 1st World Conf. Experimental Heat Transfer, Fluid Mechanics and Thermodynamics* Dubrovnik, Yugoslavia, (1988).
82. Apollonov V.V., Babayants G.I., Kazakov A.A., Kishmakhov B.Sh., Prokhorov A.M., *Kvantovaya Elektron.*, 24, 869 (1997).
83. Apollonov V.V. et al., *Quantum Electron.*, 27, 850 (1997).
84. Apollonov V.V., Prokhorov A.M. et al., *Phys. Rev. A*, 58 (3), 42 (1998).
85. Apollonov V.V. et al., *Kvantovaya Elektron.*, 25, 355 (1998).
86. Apollonov V.V. et al, *Patent No. 2399130* priority date 22.01.(2007).
87. Derzhavin S.I. *Cand. Diss.* Moscow, GPI, (1988).
88. Kuz'minov V.V. *Cand. Diss.* Moscow, GPI, (2002).
89. Schul'ts A.N. *Doct. Diss.* Moscow, LTI, (2003).
90. Apollonov V.V., Prokhorov A.M., Guenther A.H. *Laser Phys.*, 11, 930 (2001).
91. Kageyama N., Torii K., Morita T., Takauji M., Nagakura T., Maeda J., Miyajima H., Yoshida H. *Hamamatsu Photonics Report* Hamamatsu, (2011).
92. Apollonov V.V. *Natural Science*, 5, 556 (2013).
93. www.Northropgrumman.com/SolidStateHighEnergyLaserSystems/.
94. Libenson M.N., Yakovlev E.B., Shandybina G.D. *Konspekt lektsii* (Lecture Notes). Ed. by V.P. Veiko St. Petersburg: Izd ITMO, (2008).
95. Apollonov V.V., Prokhorov A.M., Guenther A.H. *Laser Focus World*, 1, 101 (2003).
96. Apollonov V.V. *Eksperlnyi Soyuz*, 3, 36 (2012).
97. Apollonov V.V. *J. Sci. Tsrael-Technol. Adv.*, 4, 3 (2012).
98. Apollonov V.V. *Chinese J. Opt.*, 6, 1 (2013).
99. Apollonov V.V. *Program of Symposium HPLS@A-2012 6*, Istanbul, (2012).